



# Reduced-order models for nonlinear vibrations of cylindrical shells via the proper orthogonal decomposition method

M. Amabili<sup>a,\*</sup>, A. Sarkar<sup>b</sup>, M. P. Paidoussis<sup>b</sup>

<sup>a</sup> *Dipartimento di Ingegneria Industriale, Università di Parma Parco Area delle Scienze 181/A, Parma 43100, Italy*

<sup>b</sup> *Department of Mechanical Engineering, McGill University, 817 Sherbrooke Street W., Montreal, Québec, Canada H3A 2K6*

Received 3 March 2003; accepted 6 June 2003

---

## Abstract

The nonlinear (large-amplitude) response of perfect and imperfect, simply supported circular cylindrical shells to harmonic excitation in the spectral neighbourhood of some of their lowest natural frequencies is investigated. The shell is assumed to be completely filled with an incompressible and inviscid fluid at rest. Donnell's nonlinear shallow-shell theory is used, and the solution is obtained by the Galerkin method. The proper orthogonal decomposition (POD) method is used to extract proper orthogonal modes that describe the system behaviour from time-series response data. These time series have been obtained via the conventional Galerkin approach (using normal modes as a projection basis) with an accurate model involving 16 degrees of freedom, validated in previous studies. The POD method, in conjunction with the Galerkin approach, permits a lower-dimensional model as compared to those obtainable via the conventional Galerkin approach. Different proper orthogonal modes computed from time series at different excitation frequencies are used and solutions are compared. Some of these sets of modes are capable of describing the system behaviour over the whole frequency range around the fundamental resonance with good accuracy and with only 3 degrees of freedom. They allow a drastic reduction in the computational effort, as compared to using the 16 degree-of-freedom model necessary when the conventional Galerkin approach is used.

© 2003 Elsevier Ltd. All rights reserved.

---

## 1. Introduction

The choice of appropriate modal expansions of the expressions for shell displacements is fundamental to guaranteeing accuracy of analytical-model results for nonlinear (large-amplitude) vibrations of circular cylindrical shells.

A complete literature review of work on the nonlinear dynamics of shells in vacuo, filled with or surrounded by quiescent or flowing fluids is given by Amabili and Paidoussis (2003). It is possible to attribute to Evensen (1967) and Dowell and Ventres (1968) the original idea of modal expansions of the shell flexural displacement involving (i) the two asymmetric modes with the same shape (sine and cosine functions around the shell circumference: one directly driven by external excitation, the driven mode; the other, normally referred to as the companion mode) and (ii) an axisymmetric term; their intuitive assumption on this was supported by the few available experimental results. The studies of Ginsberg (1973) and Chen and Babcock (1975) constitute fundamental progress in the study of the influence of the companion mode on the nonlinear forced response of circular cylindrical shells. In a recent series of papers, Amabili et al. (1999a, b, 2000a, b) systematically studied the nonlinear dynamics and large-amplitude vibrations of simply supported, circular cylindrical shells with and without quiescent or flowing fluid, by using as a basis the natural modes.

---

\*Corresponding author. Tel.: +39-0521-905896; fax: +39-0521-905705.  
E-mail address: marco@me.unipr.it (M. Amabili).

In particular, the convergence of the solution with the type of terms included in the expansion was studied in references (1999b, 2000a) and, with more terms, by Pellicano et al. (2002). In Pellicano et al. (2002) a parametric study was also performed to investigate the transition from softening type to hardening type nonlinearity. Amabili (2003a) investigated the effect of geometric imperfections and compared calculations and experiments by validating the theory.

More accurate shell theories have been used by Amabili (2003b) to study the same problem. Results show that, for water-filled shells, Donnell's shallow-shell theory gives reasonably accurate results. Other recent contributions are by Gonçalves and Batista (1988), Lakis et al. (1998), Kubenko and Koval'chuk (1998) and Jansen (2002).

In the present study, the nonlinear (large-amplitude) response of perfect and imperfect, simply supported circular cylindrical shells to harmonic excitation in the spectral neighbourhood of some of the lowest natural frequencies is investigated. The shell is assumed to be completely filled with an incompressible and inviscid fluid at rest. Donnell's nonlinear shallow-shell theory is used, and the solution is obtained by the Galerkin method. The proper orthogonal decomposition (POD) method, also referred to as the Karhunen-Loève method (Zahorian and Rothenberg, 1981; Aubry et al. 1988; Sirovich, 1987; Breuer and Sirovich, 1991; Azeez and Vakakis, 2001), is used to extract proper orthogonal modes from the system time-response, in order to describe the shell behaviour with a low-dimensional model around the fundamental resonance of the system. The shell time-responses have initially been obtained by a conventional Galerkin approach with an accurate model involving 16 degrees of freedom, previously developed by Amabili (2003a). Then, different reduced models have been developed from proper orthogonal modes extracted from response time series at different excitation frequencies. A model with 3 degrees of freedom has been built by using the POD method and it describes the shell response over the full frequency range around the fundamental resonance with very good accuracy. It allows the drastic reduction of the computational effort as compared with the original 16 degree-of-freedom model necessary with the conventional Galerkin approach.

## 2. Equation of motion and boundary conditions for the shell

A cylindrical coordinate system ( $O; x, r, \theta$ ) is chosen, with the origin  $O$  placed at the centre of one end of the shell. The displacements of points of the middle surface of the shell are denoted by  $u, v$  and  $w$ , in the axial, circumferential and radial directions, respectively;  $w$  is taken positive inwards, as shown in Fig. 1. Initial imperfections of the circular cylindrical shell associated with zero initial tension are denoted by an inward radial displacement  $w_0$ ; only radial initial imperfections are considered. By using Donnell's nonlinear shallow-shell theory, the equation of motion for finite-amplitude transverse dynamic deformation of a thin, imperfect, circular cylindrical shell is given by (Dowell and Ventres, 1968; Chen and Babcock, 1975; Amabili, 2003a)

$$D\nabla^4 w + c\dot{w} + \rho h\ddot{w} = f - p + \frac{1}{R} \frac{\partial^2 F}{\partial x^2} + \frac{1}{R^2} \left[ \frac{\partial^2 F}{\partial \theta^2} \left( \frac{\partial^2 w}{\partial x^2} + \frac{\partial^2 w_0}{\partial x^2} \right) - 2 \frac{\partial^2 F}{\partial x \partial \theta} \left( \frac{\partial^2 w}{\partial x \partial \theta} + \frac{\partial^2 w_0}{\partial x \partial \theta} \right) + \frac{\partial^2 F}{\partial x^2} \left( \frac{\partial^2 w}{\partial \theta^2} + \frac{\partial^2 w_0}{\partial \theta^2} \right) \right], \quad (1)$$

where  $D = Eh^3/[12(1 - \nu^2)]$  is the flexural rigidity,  $E$  the Young's modulus,  $\nu$  the Poisson ratio,  $h$  the shell thickness,  $R$  the mean shell radius,  $\rho$  the mass density of the shell,  $c$  the coefficient of viscous damping,  $p$  the radial pressure applied to the surface of the shell exerted by the contained fluid, and  $f$  is an external modal excitation of unspecified physical

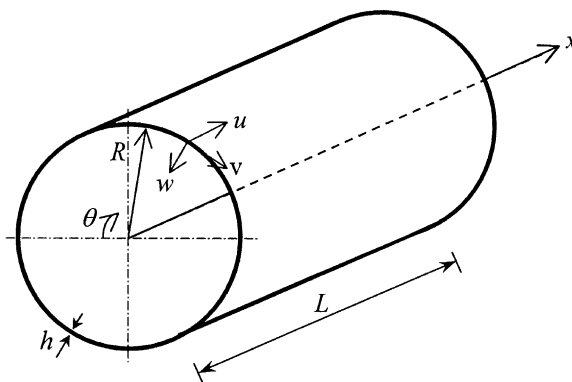


Fig. 1. Shell geometry and coordinate system.

origin, which has the form:

$$f = f_{1,m} \cos(n\theta) \sin(\pi x/L) \cos(\omega t), \tag{2}$$

where  $f_{1,m}$  is a coefficient having dimensions of pressure. Excitations with frequency close to the natural frequency of the lowest modes of the shell are considered; low-frequency modes are associated with predominantly radial motion and are identified by the pair  $(m, n)$ , where  $m$  is the number of axial half-waves and  $n$  is the number of circumferential waves. The viscous damping model introduced in Eq. (1) is unrealistic; it will be replaced by modal damping coefficients, experimentally identified, in the equations of motion as shown in Section 6. Replacement of modal excitation with a realistic point excitation will also be discussed in Section 6.

In Eq. (1) the overdot denotes a time derivative and  $F$  is the in-plane Airy stress function. Here  $F$  is given by the following compatibility equation (Dowell and Ventres, 1968; Chen and Babcock, 1975; Amabili, 2003a):

$$\frac{1}{Eh} \nabla^4 F = -\frac{1}{R} \frac{\partial^2 w}{\partial x^2} + \frac{1}{R^2} \left[ \left( \frac{\partial^2 w}{\partial x \partial \theta} \right)^2 + 2 \frac{\partial^2 w}{\partial x \partial \theta} \frac{\partial^2 w_0}{\partial x \partial \theta} - \left( \frac{\partial^2 w}{\partial x^2} + \frac{\partial^2 w_0}{\partial x^2} \right) \frac{\partial^2 w}{\partial \theta^2} - \frac{\partial^2 w}{\partial x^2} \frac{\partial^2 w}{\partial \theta^2} \right]. \tag{3}$$

In Eqs. (1) and (3), the biharmonic operator is defined as  $\nabla^4 = [\partial^2/\partial x^2 + \partial^2/(R^2 \partial \theta^2)]^2$ . Donnell’s nonlinear shallow-shell equations are accurate only for modes with a large number  $n$  of circumferential waves; it is generally assumed that  $1/n^2 \ll 1$  is required in order to have fairly good accuracy (i.e.  $n \geq 4$ ). Donnell’s nonlinear shallow-shell equations are obtained by neglecting the in-plane inertia, transverse shear deformation and rotary inertia, giving accurate results only for very thin shells. In-plane displacements are assumed to be infinitesimal, whereas  $w$  is of the same order as the shell thickness.

The forces per unit length in the axial and circumferential directions, as well as the shear force, are given by (Dowell and Ventres, 1968)

$$N_x = \frac{1}{R^2} \frac{\partial^2 F}{\partial \theta^2}, \quad N_\theta = \frac{\partial^2 F}{\partial x^2}, \quad N_{x\theta} = -\frac{1}{R} \frac{\partial^2 F}{\partial x \partial \theta}. \tag{4}$$

The force–displacement relations are (Amabili, 2003a):

$$(1 - \nu^2) \frac{N_x}{Eh} = -\frac{\nu w}{R} + \frac{1}{2} \left( \frac{\partial w}{\partial x} \right)^2 + \frac{\partial w}{\partial x} \frac{\partial w_0}{\partial x} + \frac{\nu}{2} \left( \frac{\partial w}{R \partial \theta} \right)^2 + \nu \frac{\partial w}{R \partial \theta} \frac{\partial w_0}{R \partial \theta} + \frac{\partial u}{\partial x} + \frac{\nu}{R} \frac{\partial v}{\partial \theta}, \tag{5}$$

$$(1 - \nu^2) \frac{N_\theta}{Eh} = -\frac{w}{R} + \frac{\nu}{2} \left( \frac{\partial w}{\partial x} \right)^2 + \nu \frac{\partial w}{\partial x} \frac{\partial w_0}{\partial x} + \frac{1}{2} \left( \frac{\partial w}{R \partial \theta} \right)^2 + \frac{\partial w}{R \partial \theta} \frac{\partial w_0}{R \partial \theta} + \nu \frac{\partial u}{\partial x} + \frac{1}{R} \frac{\partial v}{\partial \theta}, \tag{6}$$

$$(1 - \nu^2) \frac{N_{x\theta}}{Eh} = 2(1 - \nu) \left[ \frac{1}{R} \frac{\partial w}{\partial x} \frac{\partial w}{\partial \theta} + \frac{1}{R} \frac{\partial w}{\partial x} \frac{\partial w_0}{\partial \theta} + \frac{1}{R} \frac{\partial w_0}{\partial x} \frac{\partial w}{\partial \theta} + \frac{1}{R} \frac{\partial u}{\partial \theta} + \frac{\partial v}{\partial x} \right]. \tag{7}$$

In this study, attention is focused on a finite, simply supported, circumferentially closed circular cylindrical shells of length  $L$ . The following out-of-plane boundary conditions are imposed:

$$w = w_0 = 0, \tag{8a}$$

$$M_x = -D \{ (\partial^2 w / \partial x^2) + \nu [\partial^2 w / (R^2 \partial \theta^2)] \} = 0 \tag{8b}$$

and

$$\partial^2 w_0 / \partial x^2 = 0 \quad \text{at} \quad x = 0, L, \tag{8c}$$

where  $M_x$  is the bending moment per unit length. The in-plane boundary conditions are

$$N_x = 0 \quad \text{and} \quad v = 0 \quad \text{at} \quad x = 0, L. \tag{9a, b}$$

Moreover,  $u$ ,  $v$  and  $w$  must be continuous in  $\theta$ .

### 3. Modal expansion

Previous studies have shown that a linear modal base is the simplest choice for discretizing the system (Amabili et al., 1999a, 2000a; Pellicano et al., 2002). In particular, in order to reduce the number of degrees of freedom, it is important to use only the most significant modes. In addition to the asymmetric mode directly driven into vibration by the excitation (driven mode) it is necessary to consider (i) the orthogonal mode having the same shape and natural frequency but rotated by  $\pi/(2n)$  (companion mode), (ii) additional asymmetric modes, and (iii) axisymmetric modes. In

fact, it has clearly been established that, for large-amplitude shell vibrations, the deformation of the shell involves significant axisymmetric oscillations inwards. According to these considerations, the radial displacement  $w$  is expanded by using the eigenmodes of the empty shell which are unchanged for the completely filled shell (Amabili, 2003a):

$$w(x, \theta, t) = \sum_{m=1}^3 \sum_{k=1}^3 [A_{m,kn}(t) \cos(kn\theta) + B_{m,kn}(t) \sin(kn\theta)] \sin(\lambda_m x) + \sum_{m=1}^4 A_{(2m-1),0}(t) \sin(\lambda_{(2m-1)} x), \quad (10a)$$

where  $n$  is the number of circumferential waves,  $m$  is the number of longitudinal half-waves (only odd values are used for symmetry),  $\lambda_m = m\pi/L$ , and  $t$  is the time;  $A_{m,n}(t)$ ,  $B_{m,n}(t)$  and  $A_{m,0}(t)$  are the generalized coordinates that are unknown functions of  $t$ . The number of degrees of freedom used in the present numerical calculations is 16.

The presence of pairs of modes having the same shape but different angular orientations, the first one described by  $\cos(n\theta)$  (driven mode for the excitation given by Eq. (2)) and the other by  $\sin(n\theta)$  (companion mode), in the periodic response of the shell leads to the appearance of travelling-wave vibration around the shell in the azimuthal direction when both modes are active and when they have a relative time shift. This phenomenon is related to the axial symmetry of the system.

When the excitation has a frequency close to the resonance of a particular mode, say ( $m = 1, n$ ), results show that (i) the generalized coordinates  $A_{1,n}(t)$  and  $B_{1,n}(t)$  have the same frequency as the excitation, (ii) the coordinates  $A_{1,2n}(t)$ ,  $B_{1,2n}(t)$ ,  $A_{3,2n}(t)$ ,  $B_{3,2n}(t)$  and all the coordinates associated to axisymmetric modes have twice the frequency of the excitation, and (iii) the coordinates  $A_{3,n}(t)$ ,  $B_{3,n}(t)$ ,  $A_{1,3n}(t)$ ,  $B_{1,3n}(t)$ ,  $A_{3,3n}(t)$  and  $B_{3,3n}(t)$  have three times the frequency of the excitation.

In order to simplify the notation, Eq. (10a) is re-written in the following compact form:

$$w(x, \theta, t) = \sum_{m=1}^M \sum_{n=0}^N [A_{m,n}(t) \cos(n\theta) + B_{m,n}(t) \sin(n\theta)] \sin(\lambda_m x), \quad (10b)$$

where  $M$  and  $N$  are integers indicating the number of terms used in this expansion.

The initial radial imperfection  $w_0$  is expanded in the same form of  $w$ , i.e. in a double Fourier series satisfying boundary conditions (8a,c) at the shell edges,

$$w_0(x, \theta) = \sum_{m=1}^{\tilde{M}} \sum_{n=0}^{\tilde{N}} [\tilde{A}_{m,n} \cos(n\theta) + \tilde{B}_{m,n} \sin(n\theta)] \sin(\lambda_m x), \quad (11)$$

where  $\tilde{A}_{m,n}$  and  $\tilde{B}_{m,n}$  are the modal amplitudes of the imperfections;  $\tilde{N}$  and  $\tilde{M}$  indicate the number of terms in the expansion.

#### 4. Fluid–structure interaction

The contained fluid is assumed to be incompressible, inviscid and irrotational, so that potential theory can be used to describe fluid motion. Liquid-filled shells vibrating in the low-frequency range satisfy the incompressibility hypothesis very well. Nonlinear effects in the dynamic pressure and in the boundary conditions at the fluid–structure interface are neglected. The shell prestress due to the fluid weight is also neglected. The fluid motion is described by the velocity potential  $\Phi$ , which satisfies the Laplace equation (Gonçalves and Batista, 1988; Amabili, 2003a). Cavitation is assumed not to occur at the fluid–shell interface, and both ends of the fluid volume (corresponding to the shell edges) are assumed to be open, so that a zero pressure is assumed there. The dynamic pressure  $p$  exerted by the contained fluid on the shell is given by (Amabili, 2003a)

$$p = \rho_F (\dot{\Phi})_{r=R} = \sum_{m=1}^M \sum_{n=1}^N \rho_F [\ddot{A}_{m,n}(t) \cos(n\theta) + \ddot{B}_{m,n}(t) \sin(n\theta)] \frac{I_n(\lambda_m R)}{\lambda_m I'_n(\lambda_m R)} \sin(\lambda_m x), \quad (12)$$

where  $\rho_F$  is the mass density of the internal fluid,  $I_n$  is the modified Bessel function of order  $n$  and  $I'_n$  its derivative with respect to the argument. Eq. (12) shows that the inertial effects due to the fluid are different for each mode of the expansion. Hence, the fluid is expected to change the nonlinear behaviour of the fluid-filled shell, as a consequence of the fundamental interaction among asymmetric and the axisymmetric modes. Usually the inertial effect of the fluid is larger for axisymmetric modes, thus enhancing the nonlinear softening type behaviour of the shell.

### 5. Conventional Galerkin solution

Expansion (10) used for the radial displacement  $w$  satisfies identically the boundary conditions given by Eqs. (8a,b); moreover, it satisfies exactly the continuity of the circumferential displacement. The boundary conditions for the in-plane displacements, Eqs. (9a,b), give very complex expressions when transformed into equations involving  $w$ . Therefore, they are modified into simpler integral expressions that satisfy Eqs. (9a,b) *on an average* (Dowell and Ventres, 1968; Amabili et al., 1999a).

When the expansions of  $w$  and  $w_0$ , Eqs. (10) and (11), are substituted on the right-hand side of Eq. (3), a partial differential equation for the stress function  $F$  is obtained, composed of the homogeneous and the particular solution.

By use of the Galerkin method, 16 second-order, ordinary, coupled nonlinear differential equations are obtained for the variables  $A_{m,kn}(t)$ ,  $B_{m,kn}(t)$  and  $A_{m,0}(t)$ , for  $m = 1, \dots, M$  and  $k = 1, \dots, 3$ , by successively weighting the original Eq. (1) with the functions that describe the shape of the modes retained in Eq. (10). These equations have very long expressions containing quadratic and cubic nonlinear terms and are studied using both (i) the software AUTO 97 (Doedel et al., 1998) for continuation and bifurcation analysis of nonlinear ordinary differential equations, and (ii) direct integration of the equations of motion by using the DIVPAG routine of the Fortran library IMSL. The software AUTO 97 is capable of continuation of the solution, bifurcation analysis and branch switching by using arc-length continuation and collocation methods. In particular, the shell response under harmonic excitation has been studied by using an analysis in two steps: (i) first the excitation frequency has been fixed far enough from resonance, and the magnitude of the excitation used as bifurcation parameter; the solution has been started at zero force, where the solution is the trivial undisturbed configuration of the shell, and it has been continued up to the desired force magnitude; (ii) when the desired magnitude of excitation has been reached, the solution has been continued by using the excitation frequency as bifurcation parameter.

### 6. Proper orthogonal decomposition (POD) method

As discussed in the previous section, a Galerkin procedure, employing any set of basis functions  $\varphi_i$ , approximates the nonlinear partial differential equation (PDE) into a finite set of coupled ordinary differential equations (ODEs), with the solution being expressed as

$$w(\xi, t) = \sum_{i=1}^K q_i(t)\varphi_i(\xi), \tag{13}$$

where  $t$  is time,  $\xi$  is the vector of spatial coordinate  $(x, \theta)$  describing the shell middle surface  $\Omega$ ,  $q_i(t)$  are the generalized co-ordinates and  $K$  is the number of degrees of freedom (dofs), i.e. the number of basis functions assumed. Next, the proper orthogonal modes (also referred to as spatially coherent modes) obtained by the POD method will be used as a basis in conjunction with the Galerkin approach.

The POD method optimally extracts the spatial information necessary to characterize the spatio-temporal complexity and inherent dimension of a system, from a set of temporal snapshots of the response, gathered from either numerical simulations or experimental data (Zahorian and Rothenberg, 1981; Aubry et al., 1988; Sirovich, 1987; Breuer and Sirovich, 1991; Azeez and Vakakis, 2001; Sarkar and Païdoussis, 2003). In the present context, the temporal responses are obtained via conventional Galerkin simulations. It can be observed here that, for large-amplitude experimentally measured vibration, responses can be highly noise polluted. The solution can be expressed by using the base of the proper orthogonal modes  $\psi(\xi)$ ,

$$w(\xi, t) = \sum_{i=1}^{\tilde{K}} a_i(t)\psi_i(\xi), \tag{14}$$

where  $a_i$  are the proper orthogonal coordinates and  $\tilde{K}$  is the number of degrees of freedom of the POD solution (in general, significantly lower than  $K$ ).

The displacement field  $w$  is divided into its time-mean value  $\bar{w}(\xi)$  and the zero-mean response  $\tilde{w}(\xi, t) = (w(\xi, t) - \bar{w}(\xi))$ . In the POD method, the proper orthogonal modes are obtained by minimizing the objective function

$$\tilde{\lambda} = \langle (\psi(\xi) - \tilde{w}(\xi, t))^2 \rangle \quad \forall \xi \in \Omega \tag{15}$$

with  $\langle \rangle$  denoting the time-averaging operation. If the temporal snapshots of  $\tilde{w}$  are denoted by  $\{\tilde{w}_n\}$ , the time-averaging operation of a series of  $N$  snapshots is  $\langle \tilde{w}(\xi, t) \rangle = (1/N) \sum_{n=1}^N \tilde{w}_n(\xi)$ . By assuming  $\tilde{w}$  to be a random field, imposing  $\int_{\Omega} \psi^2(\xi) d\xi = 1$ , and developing the squared expression in Eq. (15), the proper orthogonal modes are obtained

by maximizing the quantity  $\langle \int_{\Omega} \psi(\xi) \tilde{w}(\xi, t) d\xi \rangle$  for any  $\xi$  of  $\Omega$ . To ensure that this quantity be positive, maximization of  $\langle \int_{\Omega} (\psi(\xi) \tilde{w}(\xi, t))^2 d\xi \rangle$  is performed. Therefore, the minimization of the objective function in Eq. (14) can be replaced by the maximization of the objective function

$$\lambda = \frac{\langle \int_{\Omega} (\psi(\xi) \tilde{w}(\xi, t))^2 d\xi \rangle}{\int_{\Omega} \psi^2(\xi) d\xi} \quad (16)$$

with respect to  $\psi(\xi)$ . In Eq. (16) the denominator is equal to unity. Maximization of the objective function (16) is obtained by solving the following eigenvalue problem:

$$\int_{\Omega} \langle \tilde{w}(\xi, t) \tilde{w}(\xi', t) \rangle \psi(\xi') d\xi' = \lambda \psi(\xi), \quad (17)$$

where  $\langle \tilde{w}(\xi, t) \tilde{w}(\xi', t) \rangle$  is the time-averaged spatial autocorrelation function.

A Galerkin projection scheme for determining proper orthogonal modes semi-analytically, and in parallel to approximate the solution of the PDE, is presented next. The proper orthogonal modes are projected on the eigenmodes  $\varphi(\xi)$  of the empty shell as

$$\psi(\xi) = \sum_{i=1}^K \alpha_i \varphi_i(\xi), \quad (18)$$

where  $\alpha_i$  are unknown coefficients. By substituting Eqs. (13) and (18) into Eq. (17), the following expression is obtained:

$$\sum_{i=1}^K \varphi_i(\xi) \sum_{j=1}^K \sum_{k=1}^K \langle \tilde{q}_i(t) \tilde{q}_j(t) \rangle \alpha_k \int_{\Omega} \varphi_j(\xi') \varphi_k(\xi') d\xi' = \lambda \sum_{i=1}^K \alpha_i \varphi_i(\xi), \quad (19)$$

where  $\tilde{q}_i = (q_i - \bar{q}_i)$  is the zero-mean response of the  $i$ th generalized coordinate, with  $\bar{q}_i$  being its mean. Eq. (19) is multiplied by  $\varphi_m(\xi)$  and integrated over  $\Omega$  for any  $m$  from 1 to  $K$ . By using the orthogonality relationships of the basis functions  $\varphi_m(\xi)$ , the following eigenvalue problem is finally obtained

$$\mathbf{A}\boldsymbol{\alpha} = \lambda \mathbf{B}\boldsymbol{\alpha}, \quad (20)$$

where

$$A_{ij} = \tau_i \tau_j \langle \tilde{q}_i(t) \tilde{q}_j(t) \rangle, \quad B_{ij} = \tau_i \delta_{ij}, \quad \tau_i = \int_{\Omega} \varphi_i^2(\xi) d\xi \quad (21-23)$$

and  $\delta_{ij}$  is the Kronecker delta. The norm of the basis functions  $\tau_i$  in the present case is  $\pi RL/2$  for asymmetric modes and  $\pi RL$  for axisymmetric modes; without effect on the results, they can be assumed to be 0.5 and 1, respectively. In Eq. (20),  $\mathbf{A}$  and  $\mathbf{B}$  are symmetric and positive definite matrices of dimension  $K \times K$ , and  $\boldsymbol{\alpha}$  is a vector containing the  $K$  unknown coefficients of the proper orthogonal modes. The eigenvectors  $\boldsymbol{\alpha}$  corresponding to the largest eigenvalues (known as dominant proper orthogonal modes) in Eq. (20) can now be inserted in Eq. (18) that gives a basis for the approximate solution of the PDE using the Galerkin approach; this will be referred to as the POD-Galerkin scheme hereafter. The optimal number of terms  $\tilde{K}$  to be retained can be estimated by  $\sum_{i=1}^{\tilde{K}} \lambda_i / \sum_{i=1}^K \lambda_i \geq 0.999$  in Eq. (20); however, for each problem this cut-off value can be different. It can be useful to check the convergence of the solution by increasing the value  $\tilde{K}$ ; over a certain value, results become less accurate, because the additional terms introduced in the expansion are highly noise-polluted. As mentioned previously, the order of the POD-Galerkin model necessary to capture the salient dynamical features of the original PDE is significantly lower than that of the conventional Galerkin model.

In some applications, it may be better to use time responses obtained for different system parameters in order to produce better proper orthogonal modes. For example, in the case of two such responses, Eq. (20) is still used, but Eq. (21) is replaced by

$$\mathbf{A} = \frac{p_1 \mathbf{A}^{(1)}}{|\mathbf{A}^{(1)}|} + \frac{p_2 \mathbf{A}^{(2)}}{|\mathbf{A}^{(2)}|}, \quad (24)$$

where  $|\mathbf{A}| = \sqrt{\text{Tr}(\mathbf{A}\mathbf{A}^T)}$  is the Frobenius norm of  $\mathbf{A}$ ,  $\text{Tr}$  gives the trace of the matrix,

$$A_{ij}^{(1)} = \tau_i \tau_j \langle \tilde{q}_i^{(1)}(t) \tilde{q}_j^{(1)}(t) \rangle, \quad (25)$$

$$A_{ij}^{(2)} = \tau_i \tau_j \langle \tilde{q}_i^{(2)}(t) \tilde{q}_j^{(2)}(t) \rangle \quad (26)$$

and  $\tilde{q}_i^{(1)}(t)$  and  $\tilde{q}_i^{(2)}(t)$  are the zero-mean first and second responses, respectively. In Eq. (24)  $p_1$  and  $p_2$  are two coefficients used to give a different weight to the first and second response in the calculation of the proper orthogonal modes; the Frobenius norm is introduced just to normalize the matrices, as the amplitude of the generalized coordinates  $q_i(t)$  can be very different for the two responses.

### 7. Galerkin solution with proper orthogonal modes

By using Eqs. (10), (14) and (18), the expansion used for the POD solution is given by

$$w(\xi, t) = \sum_{i=1}^{\tilde{K}} a_i(t) \sum_{j=1}^{\tilde{K}} \alpha_{j,i} \varphi_j(\xi) = \sum_{i=1}^{\tilde{K}} a_i(t) \sum_{m=1}^M \sum_{n=0}^N [\alpha_{m,n,i} \cos(n\theta) + \beta_{m,n,i} \sin(n\theta)] \sin(\lambda_m x), \tag{27}$$

where on the right-hand side two different symbols,  $\alpha$  and  $\beta$ , have been introduced to differentiate the coefficients of the proper orthogonal modes for cosine and sine terms in  $\theta$ . Expression (27) satisfies identically the boundary conditions given by Eqs. (8a,b); moreover, it satisfies exactly the continuity of the circumferential displacement (Amabili, 2003a)

$$\int_0^{2\pi} \partial v / \partial \theta \, d\theta = v(2\pi) - v(0) = 0 \tag{28}$$

as can be verified after calculation of the stress function  $F$  from Eq. (3).

For the same reasons discussed in Section 5, in this case also Eqs. (9a,b) are replaced by simpler integral expressions that satisfy these boundary conditions *on an average* (Dowell and Ventres, 1968). Specifically, the following conditions are imposed:

$$\int_0^{2\pi} N_x R \, d\theta = 0 \quad \text{at } x = 0, L, \quad \int_0^{2\pi} \int_0^L N_{x\theta} \, dx R \, d\theta = 0. \tag{29, 30}$$

Eq. (29) ensures a zero axial force  $N_x$  on an average at  $x = 0, L$ ; Eq. (30) is satisfied when  $v = 0$  on an average at  $x = 0, L$ ; and  $u$  is continuous in  $\theta$  on an average. Substitution of Eqs. (9a,b) by Eqs. (29) and (30) simplifies computations, although it introduces an approximation (boundary conditions (9a,b) are exactly satisfied at  $n$  discrete points, where  $n$  is the number of circumferential waves).

When the expansion of  $w$  is substituted in the right-hand side of Eq. (3) and zero initial imperfection is assumed ( $w_0 = 0$ ), a partial differential equation for the stress function  $F$  is obtained; the solution may be written as

$$F = F_h + F_p, \tag{31}$$

where  $F_h$  is the homogeneous solution and  $F_p$  the particular solution. The particular solution is given by

$$F_p = \sum_{i=1}^{\tilde{K}} a_i(t) \sum_{m=1}^{2M} \sum_{n=0}^{2N} [F_{m,n,i,1} \sin(m\eta) \sin(n\theta) + F_{m,n,i,2} \sin(m\eta) \cos(n\theta) + F_{m,n,i,3} \cos(m\eta) \sin(n\theta) + F_{m,n,i,4} \cos(m\eta) \cos(n\theta)], \tag{32}$$

where  $\eta = \pi x/L$ , and the coefficients  $F_{m,n,i,j}$ ,  $j = 1, \dots, 4$ , have a lengthy expressions not given here for brevity. The technique used to calculate  $F_{m,n,i,j}$ ,  $j = 1, \dots, 4$ , in Eq. (32) is based on the *Mathematica* computer program (Wolfram, 1999) for symbolic manipulations. If Eq. (27) is substituted into the right-hand side of Eq. (3), after some algebra the following expressions are obtained:

$$\frac{1}{R} \frac{\partial^2 w}{\partial x^2} = \frac{\pi^2}{RL^2} \frac{\partial^2 w}{\partial \eta^2} = -\frac{\pi^2}{RL^2} \sum_{i=1}^{\tilde{K}} a_i(t) \sum_{m=1}^M \sum_{n=0}^N [\alpha_{m,n,i} \cos(n\theta) + \beta_{m,n,i} \sin(n\theta)] m^2 \sin m\eta, \tag{33}$$

$$\left( \frac{1}{R} \frac{\partial^2 w}{\partial x \partial \theta} \right)^2 = \frac{\pi^2}{R^2 L^2} \sum_{i=1}^{\tilde{K}} \sum_{j=1}^{\tilde{K}} a_i(t) a_j(t) \sum_{m_1=1}^M \sum_{m_2=1}^M \sum_{n_1=0}^N \sum_{n_2=0}^N m_1 m_2 n_1 n_2 \cos(m_1 \eta) \cos(m_2 \eta) [-\alpha_{m_1, n_1, i} \sin(n_1 \theta) + \beta_{m_1, n_1, i} \cos(n_1 \theta)] \times [-\alpha_{m_2, n_2, j} \sin(n_2 \theta) + \beta_{m_2, n_2, j} \cos(n_2 \theta)], \tag{34}$$

$$\frac{\partial^2 w}{\partial x^2} \frac{\partial^2 w}{R^2 \partial \theta^2} = \frac{\pi^2}{R^2 L^2} \sum_{i=1}^{\tilde{K}} \sum_{j=1}^{\tilde{K}} a_i(t) a_j(t) \sum_{m_1=1}^M \sum_{m_2=1}^M \sum_{n_1=0}^N \sum_{n_2=0}^N m_1^2 n_1^2 \sin(m_1 \eta) \sin(m_2 \eta) [\alpha_{m_1, n_1, i} \cos(n_1 \theta) + \beta_{m_1, n_1, i} \sin(n_1 \theta)] \times [\alpha_{m_2, n_2, j} \cos(n_2 \theta) + \beta_{m_2, n_2, j} \sin(n_2 \theta)]. \tag{35}$$

By substituting Eqs. (32)–(35) into Eq. (3), the unknown functions  $F_{m,n,i,j}$  can be identified by using the computer program *Mathematica* version 4 (Wolfram, 1999).

The homogeneous solution may be assumed to have the form (Amabili et al., 1999a; Amabili, 2003a)

$$F_h = \frac{1}{2} \bar{N}_x R^2 \theta^2 + \frac{1}{2} x^2 \left\{ \bar{N}_\theta - \frac{1}{2\pi RL} \int_0^L \int_0^{2\pi} \left[ \frac{\partial^2 F_p}{\partial x^2} \right] R \, d\theta \, dx \right\} - \bar{N}_{x\theta} x R \theta, \tag{36}$$

where  $\bar{N}_x$ ,  $\bar{N}_\theta$ , and  $\bar{N}_{x\theta}$  are the average in-plane restraint stresses (forces per unit length) generated at the shell ends, defined as

$$\bar{N}_\# = [1/(2\pi L)] \int_0^{2\pi} \int_0^L N_\# \, dx \, d\theta, \tag{37}$$

where the subscript # must be replaced by  $x$ ,  $\theta$  and  $x\theta$ , in turn. Eq. (36) is chosen in order to satisfy the boundary conditions imposed. Moreover, it satisfies Eqs. (4) on the average. Boundary conditions (29, 30) allow us to express  $\bar{N}_x$ ,  $\bar{N}_\theta$  and  $\bar{N}_{x\theta}$ , see Eqs. (5)–(7), in terms of  $w$ ,  $w_0$  and their derivatives. The expressions obtained by inserting the expansion of  $w$  given by Eq. (27) in Eqs. (5)–(7) and (37) are obtained as follows. In accord with the boundary conditions (8) and (9), it is assumed that

$$\bar{N}_x = \text{constant}; \text{ (in particular, } \bar{N}_x = 0) \text{ and } \bar{N}_{x\theta} = 0. \tag{38}$$

Consequently, after simple calculations one obtains

$$\bar{N}_\theta = v \bar{N}_x + \frac{Eh}{2\pi RL} \int_0^{2\pi} \int_0^L \left[ -\frac{w}{R} + \frac{1}{2} \left( \frac{\partial w}{R \partial \theta} \right)^2 + \frac{\partial w}{R \partial \theta} \frac{\partial w_0}{R \partial \theta} \right] dx \, R \, d\theta. \tag{39}$$

By inserting Eq. (27) and  $w_0 = 0$  into Eq. (39), the following expression is obtained:

$$\bar{N}_\theta = v \bar{N}_x + \frac{Eh}{2\pi R} \left\{ -2 \sum_{i=1}^{\tilde{K}} a_i(t) \sum_{m=1}^M \frac{\alpha_{m,0,i}}{m} [1 - (-1)^m] + \frac{\pi}{4R} \sum_{i=1}^{\tilde{K}} \sum_{j=1}^{\tilde{K}} a_i(t) a_j(t) \sum_{n=1}^N \sum_{m=1}^M n^2 (\alpha_{m,n,i} \alpha_{m,n,j} + \beta_{m,n,i} \beta_{m,n,j}) \right\}. \tag{40}$$

By use of the Galerkin method,  $\tilde{K}$  second order, ordinary, coupled nonlinear differential equations are obtained for the variables  $a_i(t)$ , for  $i = 1, \dots, \tilde{K}$  by successively weighting the single original Eq. (1) with the proper orthogonal modes  $\psi_i$  retained in Eq. (27). The Galerkin projections of the equation of motion (1) have been performed analytically by using the *Mathematica* computer software (Wolfram, 1999) in order to avoid errors arising from numerical calculations of surface integrals of trigonometric functions. The Galerkin projection of the modal excitation  $f$  on the weighting functions  $\psi_i$  gives

$$\langle f, \psi_i \rangle = \int_0^{2\pi} \int_0^L f \psi_i \, dx \, R \, d\theta = \alpha_{1,n,i} \frac{\pi RL}{2} f_{1,n} \cos(\omega t), \text{ for } i = 1, \dots, \tilde{K}. \tag{41}$$

This kind of external excitation is quite unrealistic. Practically, one or more forces are usually applied to the system. A more realistic case is the one of a harmonic point excitation, modelling for instance the excitation by an electro-dynamical exciter (shaker). For this reason, numerical results in the following section are obtained with this realistic excitation. The point force excitation  $\tilde{f}$  is the resultant of the following pressure distribution:

$$f = \tilde{f} \delta(R\theta - R\tilde{\theta}) \delta(x - \tilde{x}) \cos(\omega t), \tag{42}$$

where  $\delta$  is the Dirac delta function,  $\tilde{f}$  is the magnitude of the localized force, and  $\tilde{\theta}$  and  $\tilde{x}$  give the angular and axial coordinates of the point of application of the force, respectively. If the point excitation is located at  $\tilde{\theta} = 0$ ,  $\tilde{x} = L/2$ , the Galerkin projection of the excitation  $f$  on the weighting functions  $\psi_i$  gives

$$\langle f, \psi_i \rangle = \tilde{f} \cos(\omega t) \sum_{m=1}^M \sum_{n=0}^N \alpha_{m,n,i}. \tag{43}$$

In this case, setting  $\tilde{f} = f_{1,n} \pi R L/2$ , the only difference between modal excitation and point excitation is that the point-excitation directly drives all conventional Galerkin modes described by a cosine function in the angular direction  $\theta$  and also the axisymmetric modes, instead of only the  $(m, n)$  cosine mode.

The projection of the left-hand side terms in Eq. (1) gives

$$\langle D\nabla^4 w + chw + ph\dot{w}, \psi_i \rangle = \frac{\pi RL}{2} \sum_{m=1}^M \sum_{n=0}^N (\alpha_{m,n,i}^2 + \beta_{m,n,i}^2) \begin{pmatrix} 1 & \text{if } n > 0 \\ 2 & \text{if } n = 0 \end{pmatrix} \left[ a_i(t) D \left( \lambda_m^2 + \frac{n^2}{R^2} \right)^2 + \dot{a}_i(t) ch + \ddot{a}_i(t) ph \right]. \tag{44}$$

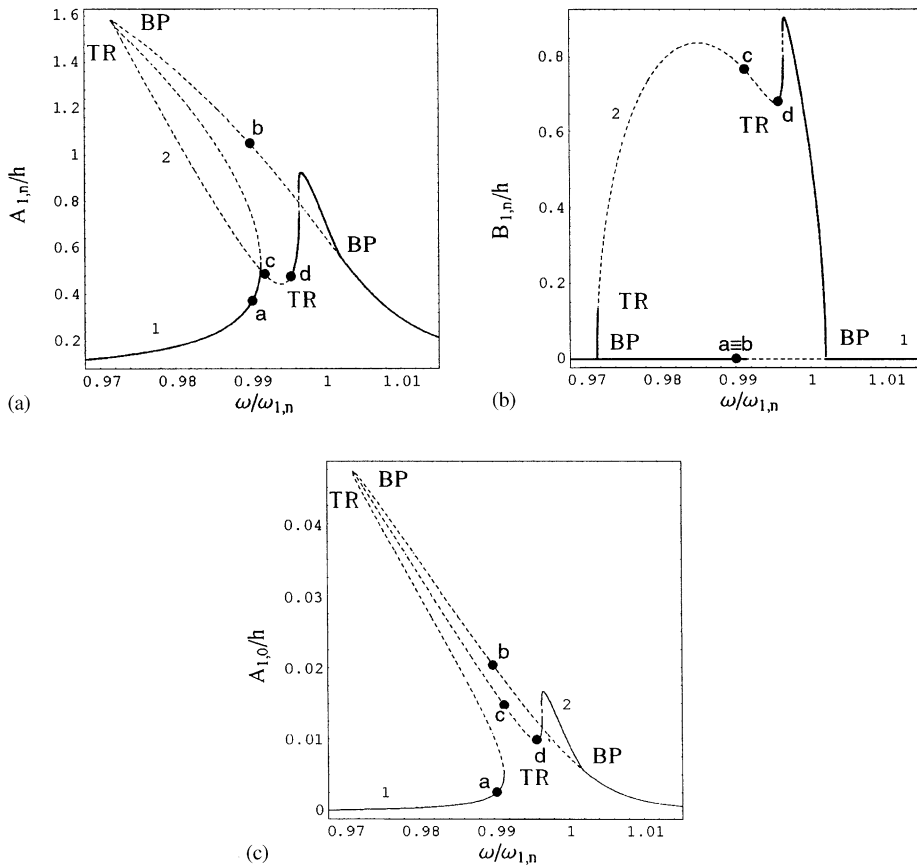


Fig. 2. Maximum amplitude of vibration versus excitation frequency; conventional Galerkin model. (a) Maximum amplitude of  $A_{1,n}(t)$ , driven mode; (b) maximum amplitude of  $B_{1,n}(t)$ , companion mode; (c) maximum amplitude of  $A_{1,0}(t)$ , first axisymmetric mode. 1, branch “1”; 2, branch “2”; BP, pitchfork bifurcation; TR, Neimark-Sacker (torus) bifurcations. —, stable solutions; ---, unstable periodic solutions; a, case “a”; b, case “b”; c, case “c”; d, case “d”.

The Galerkin projection of the fluid pressure, in the case of a fluid-filled shell, gives

$$\langle p, \psi_i \rangle = \frac{\pi RL}{2} \rho_F \sum_{m=1}^M \sum_{n=0}^N (\alpha_{m,n,i}^2 + \beta_{m,n,i}^2) \begin{pmatrix} 1 & \text{if } n > 0 \\ 2 & \text{if } n = 0 \end{pmatrix} \frac{I_n(\lambda_m R)}{\lambda_m I'_n(\lambda_m R)} \ddot{a}_i(t). \tag{45}$$

Finally, the equations of motion have the following form:

$$\begin{aligned} \ddot{a}_i(t) + 2\zeta_i \omega_i \dot{a}_i(t) + \omega_i^2 a_i(t) + \sum_{i,j=1}^{\tilde{K}} h_{ij} a_i(t) a_j(t) + \sum_{i,j,k=1}^{\tilde{K}} h_{ijk} a_i(t) a_j(t) a_k(t) \\ = \tilde{f} \cos(\omega t) \sum_{m=1}^M \sum_{n=0}^N \alpha_{m,n,i} / \mu_i \quad \text{for } i = 1, \dots, \tilde{K}, \end{aligned} \tag{46}$$

where  $h_{ij}$  and  $h_{ijk}$  are the coefficients of quadratic and cubic nonlinear terms, respectively,

$$\mu_i = \frac{\pi RL}{2} \sum_{m=1}^M \sum_{n=0}^N (\alpha_{m,n,i}^2 + \beta_{m,n,i}^2) \begin{pmatrix} 1 & \text{if } n > 0 \\ 2 & \text{if } n = 0 \end{pmatrix} \left[ \rho h + \rho_F \frac{I_n(\lambda_m R)}{\lambda_m I'_n(\lambda_m R)} \right], \tag{47}$$

$$\omega_i^2 = \frac{\pi R L}{2} \sum_{m=1}^M \sum_{n=0}^N (\alpha_{m,n,i}^2 + \beta_{m,n,i}^2) \begin{pmatrix} 1 & \text{if } n > 0 \\ 2 & \text{if } n = 0 \end{pmatrix} \left[ \left( \lambda_m^2 + \frac{n^2}{R^2} \right)^2 + \gamma_{m,n} \right] / \mu_i \tag{48}$$

$\gamma_{m,n}$  is a term associated with the projection of  $-(1/R)\partial^2 F/\partial x^2$ , and  $\zeta_i$  is the damping ratio. The damping ratio is related to the coefficient of viscous damping  $c$  by  $\zeta_i = c/(2\omega_i \mu_i)$ , where  $\omega_i$  is the natural radian frequency of the  $i$ th proper

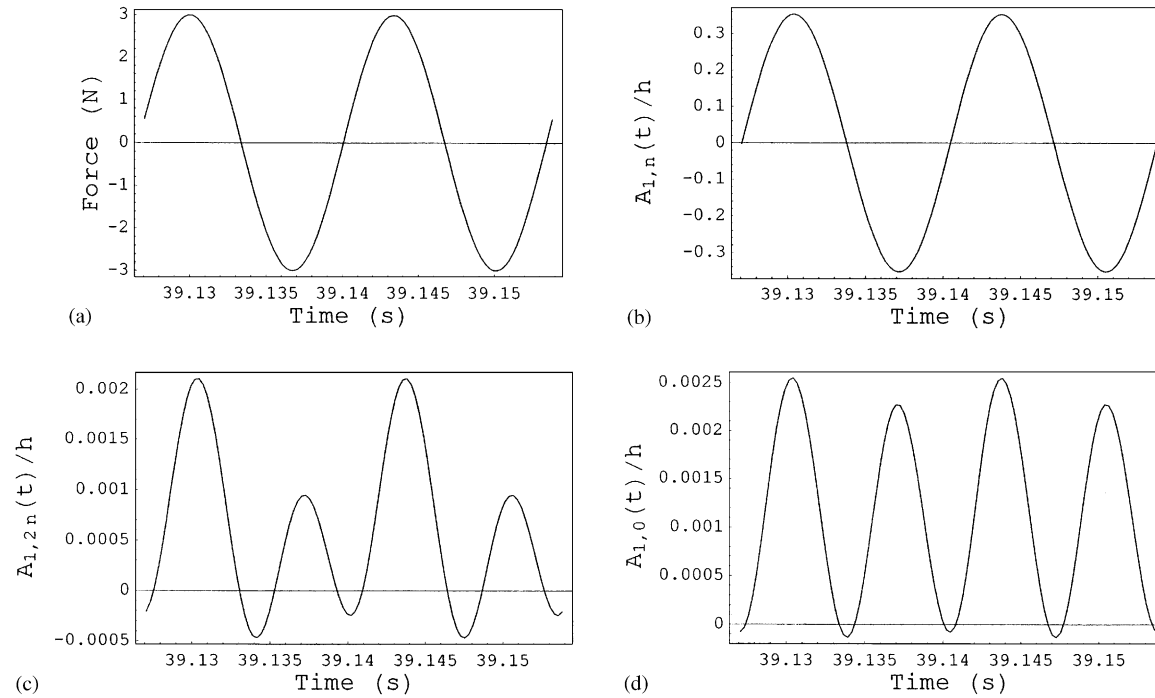


Fig. 3. Time response at excitation frequency  $\omega/\omega_{1,n} = 0.99$ , corresponding to point “a” in Fig. 2; conventional Galerkin model. (a) Harmonic force excitation; (b) modal coordinate  $A_{1,n}(t)$  associated to the driven mode; (c) modal coordinate  $A_{1,2n}(t)$ ; (d) modal coordinate  $A_{1,0}(t)$  associated to the first axisymmetric mode.

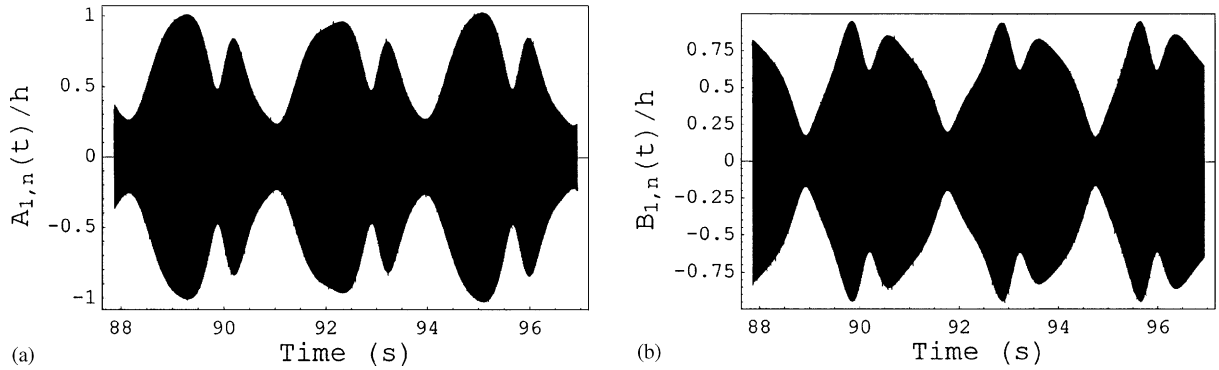


Fig. 4. Time response at excitation frequency  $\omega/\omega_{1,n}=0.991$ , corresponding to point “c” in Fig. 2; conventional Galerkin model: (a) modal coordinate  $A_{1,n}(t)$  associated to the driven mode; (b) modal coordinate  $B_{1,n}(t)$  associated to the companion mode.

orthogonal mode. In Eq. (46) modal damping and point excitation have been used. Eqs. (46) contain quadratic and cubic nonlinear terms and are studied with the same numerical techniques as described in Section 4. In particular, in the numerical simulations with the AUTO code, an artifice has been used to compare the POD and the conventional Galerkin solutions by adding a new variable  $z_j$ , with the following definition:

$$\dot{z}_j = \sum_{i=1}^{\bar{K}} \alpha_{i,j} \dot{a}_i(t) + \varepsilon z_j (1 + z_j^2) \quad (49)$$

in this way  $z_j$ , except for negligible nonlinear terms of order  $\varepsilon \cong 10^{-10}$  necessary to avoid singularity of the system, gives the conversion from proper orthogonal modes to the response of the  $j$ th conventional Galerkin mode.

## 8. Numerical results

A water-filled circular cylindrical shell (without imperfections) is considered, with the following dimensions and material properties:  $L = 520$  mm,  $R = 149.4$  mm,  $h = 0.519$  mm,  $E = 1.98 \times 10^{11}$  Pa,  $\rho = 7800$  kg/m<sup>3</sup>,  $\rho_F = 1000$  kg/m<sup>3</sup> and  $\nu = 0.3$ . Numerical calculations have been performed for the fundamental mode ( $n = 5$ ,  $m = 1$ ) of the water-filled shell, a case previously studied by Amabili (2003a). The response–frequency relationship of the fundamental mode of the perfect, water-filled shell under harmonic point excitation of magnitude 3 N at  $\tilde{x} = L/2$  and  $\tilde{\theta} = 0$  and assuming modal damping  $\zeta_{1,n} = 0.0017$  is given in Fig. 2, obtained by the conventional Galerkin approach. The natural frequency  $\omega_{1,n}$  of this mode is 77.64 Hz, according to Donnell’s theory of shells. Fig. 2 shows the main branch “1” corresponding to zero amplitude of the companion mode  $B_{1,n}(t)$ ; this branch has pitchfork bifurcations (BP) at  $\omega/\omega_{1,n} = 0.9714$  and at 1.0018 where branch “2” appears. This new branch corresponds to participation of both  $A_{1,n}(t)$  and  $B_{1,n}(t)$ , giving a travelling wave response. Branch “2” loses stability through two Neimark-Sacker (torus) bifurcations (TR), at  $\omega/\omega_{1,n} = 0.9716$  and 0.9949. No stable response is indicated in Fig. 2 for  $0.9911 < \omega/\omega_{1,n} < 0.9949$ ; in fact, only simple-periodic responses are recognized as stable solutions in Fig. 2. The response of the shell for  $0.9911 < \omega/\omega_{1,n} < 0.9949$  is still physically stable, but it is an amplitude-modulated (quasiperiodic) response.

In Fig. 2, four points, “a”, “b”, “c” and “d” are indicated at specific excitation frequencies,  $\omega/\omega_{1,n} = 0.99$ , 0.99, 0.991, 0.995, respectively. Time traces calculated for these four specific system conditions have been used to produce proper orthogonal modes, and the most significant generalized coordinates are shown in Figs. 3–5 (time trace at point “b” is not shown for brevity). Cases “a” and “b” correspond to shell vibration without companion mode participation (in particular, case “b” corresponds to an unstable response); at point “c”, the shell has a quasiperiodic response, with modulations of amplitude, and both driven and companion modes are active; at point “d”, the shell response is simple periodic with companion mode participation.

The POD method has been used to extract proper orthogonal modes from the time series. The coefficients of the proper orthogonal modes are given in Table 1 (most significant terms only) for the modes extracted for the following cases: “a”, “c”, “d”, and a combination of “b” and “d” with the same weight (see Eq. (24),  $p_1 = p_2 = 0.5$ ) and of “c” and “-c” (case “-c” is obtained by changing in case “c” the sign to the generalized coordinates associated to  $\sin(n\theta)$  terms in Eq. (10b)). The optimal number of proper orthogonal modes  $\bar{K}$  to be retained can be estimated by plotting  $\sum_{i=1}^{\bar{K}} \lambda_i / \sum_{i=1}^{\bar{K}} \lambda_i$  as a function of  $\bar{K}$ , as has been done in Figs. 6 and 7 for cases “a” and “c”, respectively. For case “a”

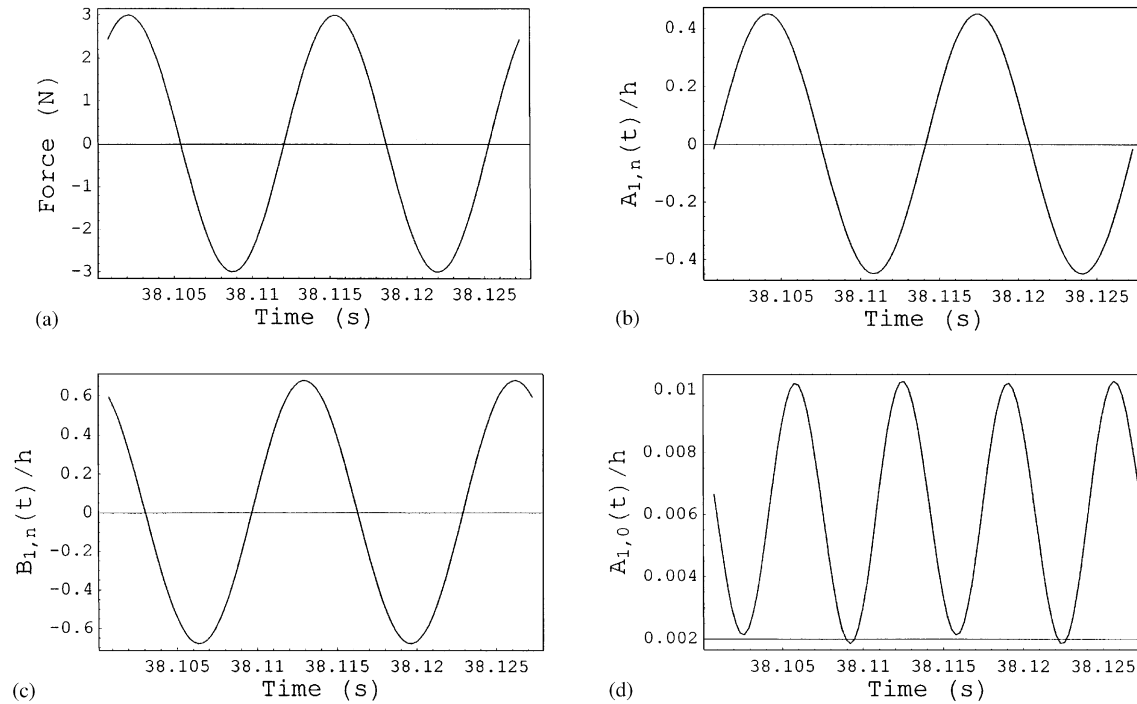


Fig. 5. Time response at excitation frequency  $\omega/\omega_{1,n} = 0.995$ , corresponding to point “d” in Fig. 2; conventional Galerkin model. (a) Harmonic force excitation; (b) modal coordinate  $A_{1,n}(t)$  associated to the driven mode; (c) modal coordinate  $B_{1,n}(t)$  associated to the companion mode; (d) modal coordinate  $A_{1,0}(t)$  associated to the first axisymmetric mode.

Table 1  
Coefficients of the proper orthogonal modes (main terms only)

Time response	$i$	$\alpha_{1,5,i}$	$\beta_{1,5,i}$	$\alpha_{1,10,i}$	$\beta_{1,10,i}$	$\alpha_{1,0,i}$	$\alpha_{3,0,i}$
“a”	1	−1	0	−0.00163	0	−0.000391	−0.00006
	2	0.001658	0	−0.5819	0	−0.7914	0.1490
“c”	1	0.9053	−0.4248	0.000140	0.000014	0.0000206	$6.91 \times 10^{-6}$
	2	−0.4248	−0.9053	−0.000216	$-5.47 \times 10^{-6}$	−0.000063	$-6.41 \times 10^{-6}$
	3	−0.000123	−0.000119	0.1813	−0.1918	0.9456	−0.1819
“d”	1	0.4271	−0.9042	−0.00014	$7.9 \times 10^{-6}$	−0.000047	$-4.59 \times 10^{-6}$
	2	−0.9042	−0.4271	−0.0016	−0.000024	−0.00038	−0.000061
	3	0.00035	0.00019	−0.4784	0.5830	0.6311	−0.1199
0.5 “b” + 0.5 “d”	1	0.9155	−0.40225	−0.000224	$-1.53 \times 10^{-6}$	−0.000088	$7.44 \times 10^{-7}$
	2	−0.40225	−0.9155	−0.000224	−0.000013	−0.000040	−0.000016
	3	−0.0001695	0.0002625	−0.44345	0.1674	−0.8611	0.1636
0.5 “c” + 0.5 “−c”	1	1	0	0.000213	0	0.0000434	$8.85 \times 10^{-6}$
	2	0	1	0	−0.000291	0	0
	3	0.000123	0	−0.1847	0	−0.9641	0.1855

the first mode has almost all the energy of the system, which is completely attained with two modes; an additional mode is necessary for case “c”.

### 8.1. Frequency domain results

The first results analysed are those with proper orthogonal modes extracted from time series “a”. The maximum amplitude of the shell response for all the frequency range in the spectral neighbourhood of the fundamental frequency is shown in Fig. 8, calculated by using two proper orthogonal modes; the previous result (Fig. 2) is also plotted for comparison. Results are converted from proper orthogonal coordinates to the more intuitive modal coordinate by introducing Eq. (49) in the AUTO computer program. Results for branch “1” are extremely close, even though the dimension of the system has been reduced from 16 to 2. In this case, the proper orthogonal modes are not able to detect the bifurcation points and branch “2”, because they have been computed by using a time response with zero companion mode participation. The convergence of the solution is investigated in Fig. 9, where the response computed with one, two and three proper orthogonal modes is shown. Results show that the additional third mode gives zero contribution to the shell response and that only two modes are necessary; results with only one mode are completely wrong. The first of the two necessary modes is associated with the driven mode ( $m = 1, n = 5$ ), while the second is associated mainly with axisymmetric oscillation involving contribution of modes with  $2n$  circumferential waves (see Table 1); the axisymmetric term is fundamental for correctly predicting the nonlinearity of the shell, as shown in previous studies (Amabili et al., 1999b, 2000a).

The maximum amplitude of the shell response is shown in Fig. 10 for case “d”, calculated by using three proper orthogonal modes. The computed response tends to follow both branches “1” and “2” of the original results but without any bifurcation point. However, the reduced order model is not particularly good over the whole of the frequency range displayed. In contrast, an excellent result is obtained with three proper orthogonal modes calculated from time response “c” in Fig. 11. In this case, Neimark-Sacker (torus) bifurcations are detected at  $\omega/\omega_{1,n} = 0.9712, 0.9942, 0.9731$  and  $0.9943$ , but pitchfork bifurcations are not. This result seems to indicate that response “c” with amplitude modulations has more information on the system dynamics than the simple periodic response “d” with companion mode participation. Results for case “c” in the original proper orthogonal coordinates are shown in Fig. 12; stability of the simple periodic response is given here. Figs. 11 and 12 show a curious loop in the solution, which is necessary for following all the branches of the solution, as a consequence of no pitchfork bifurcations having been obtained with this POD model.

In order to verify whether results for case “d” could be improved, proper orthogonal modes have been extracted by combining time series of cases “b” and “d”. The maximum amplitude of the shell response is shown in Figs. 13 and 14 for different weights of the time traces and three proper orthogonal modes. In particular, Fig. 13 has been obtained with weights 0.3 for case “b” and 0.7 for case “d”; Fig. 14 has been obtained with weights 0.5 for both cases. Both results are better than that those obtained with time trace “d” alone, and the one with equal weights of the two traces is the best, even though it is not as good as the result from case “c”. However, in this case the loop found in Fig. 11 is avoided and

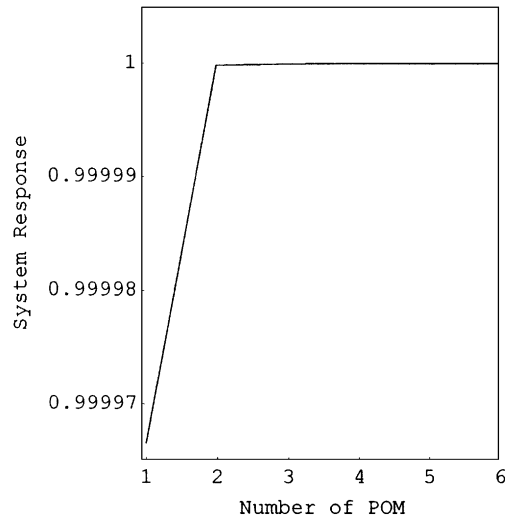


Fig. 6. Significance of POD eigenvalues versus the number of proper orthogonal modes; case “a”.

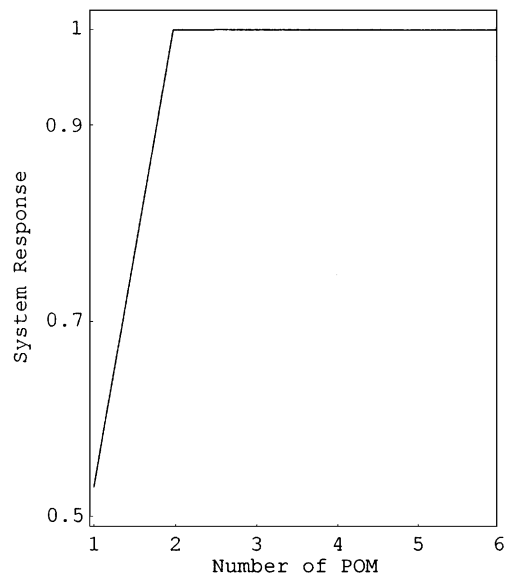


Fig. 7. Significance of POD eigenvalues versus the number of proper orthogonal modes; case “c”.

the results are more easily understandable. Results given in Fig. 14 are shown in Fig. 15 in the original proper orthogonal coordinates, also differentiating stable and unstable portions of the solution (note that the quasiperiodic solution is denoted as an “unstable solution”, to differentiate it from the stable harmonic response).

Results for case “c”, though quantitatively very good, are qualitatively unsatisfactory, because no pitchfork bifurcations are obtained. However, this is due to the fact that the symmetry in the solution of the system has inadvertently been broken by considering the travelling wave to occur in one direction only. In fact, associated with this response there is always an identical one travelling in the opposite angular direction. By taking into account both responses (the second one must be obtained from response “c” only changing the sign of the generalized coordinates associated with  $\text{Sin}(n\theta)$  terms in Eq. (10b)<sup>1</sup>) and combining them with identical weights in Eq. (24),

<sup>1</sup>If the second response is obtained by time integration, as done for the first one, numerical differences between the two responses travelling in opposite directions will appear, and the system will not fully recover its symmetry.

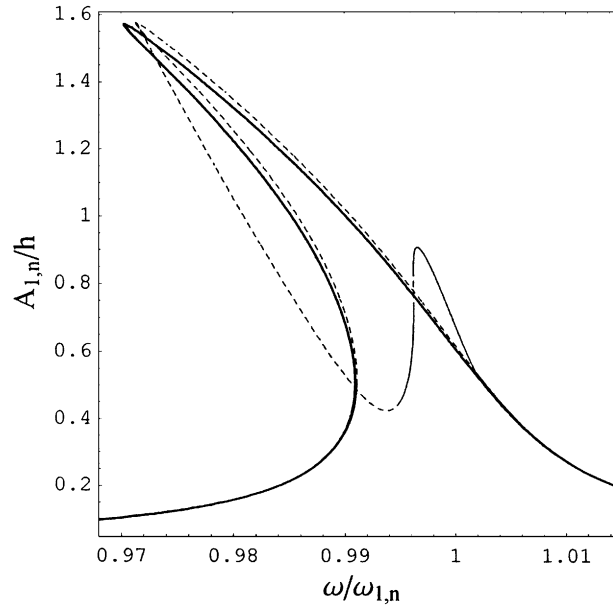


Fig. 8. Maximum amplitude of vibration versus excitation frequency; POD model versus conventional Galerkin model, case “a”. Maximum amplitude of  $A_{1,n}(t)$ , driven mode. —, POD model (2 modes); —, stable conventional Galerkin solutions; -·-, unstable conventional Galerkin solutions.

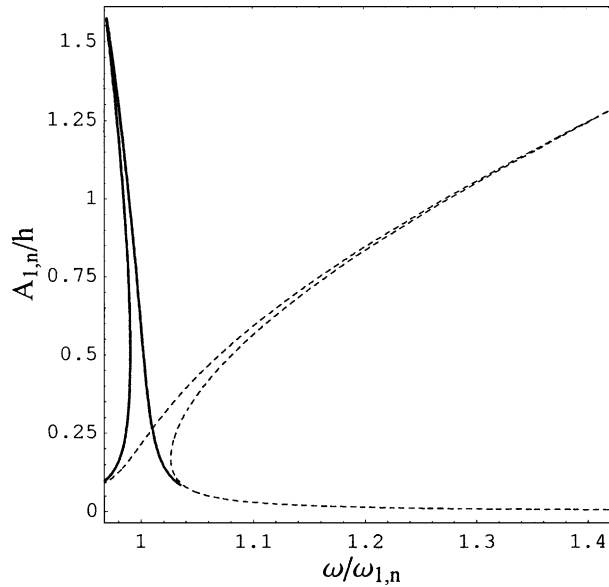


Fig. 9. Maximum amplitude of  $A_{1,n}(t)$  versus excitation frequency; POD model, case “a”. —, POD model with 3 modes; —, POD model with 2 modes (coincident with model with 3 modes); -·-, POD model with 1 mode.

the symmetry of the system is recovered; then both pitchfork and Neimark-Sacker (torus) bifurcations are obtained. The results of this reduced order model (with three proper orthogonal modes) are given in Fig. 16, where comparison to the original results is seen to be very satisfactory. Results for case “c” combined with “-c” in the original proper orthogonal coordinates are shown in Fig. 17; in this case, stable and unstable periodic solutions are clearly identified.

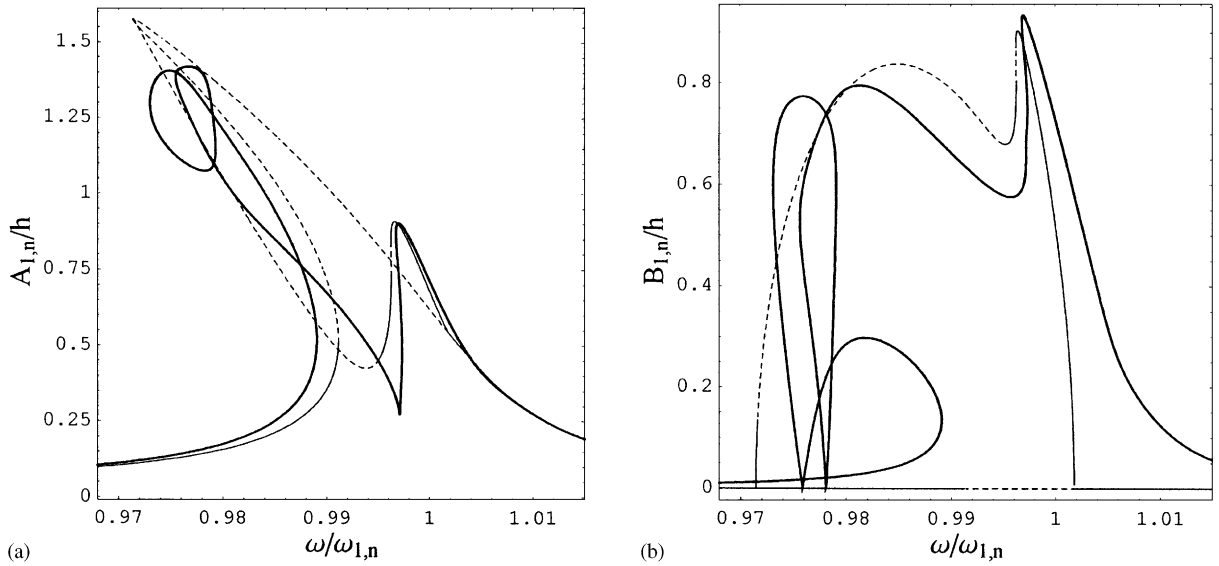


Fig. 10. Maximum amplitude of vibration versus excitation frequency; POD model versus conventional Galerkin model, case “d”. (a) Maximum amplitude of  $A_{1,n}(t)$ , driven mode; (b) maximum amplitude of  $B_{1,n}(t)$ , companion mode. —, POD model (3 modes); —, stable conventional Galerkin solutions; ---, unstable conventional Galerkin solutions.

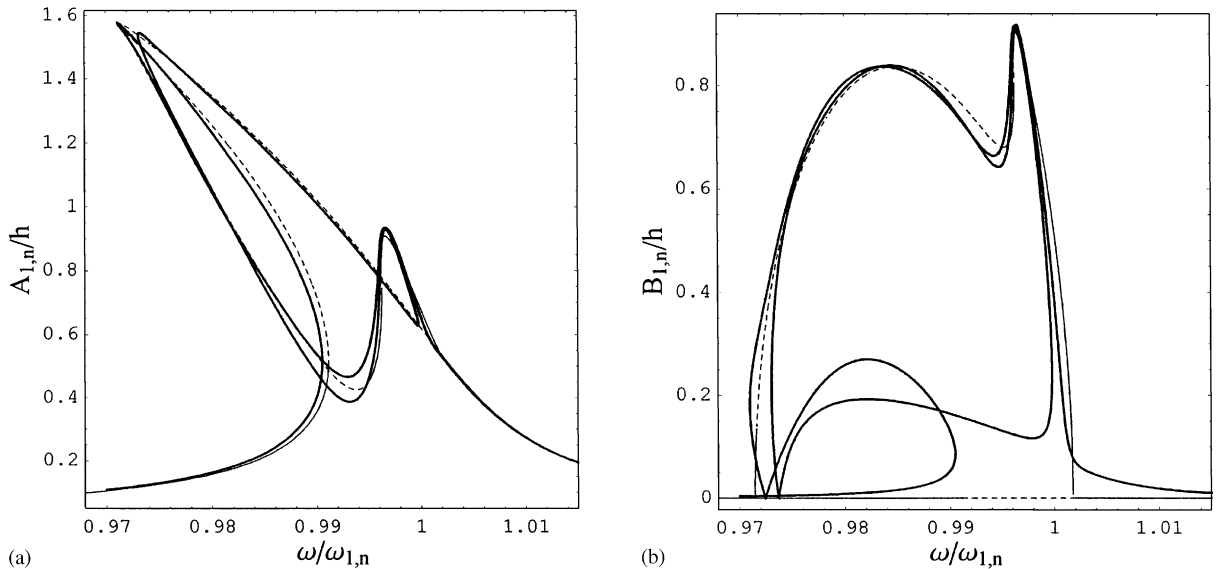


Fig. 11. Maximum amplitude of vibration versus excitation frequency; POD model versus conventional Galerkin model, case “c”. (a) Maximum amplitude of  $A_{1,n}(t)$ , driven mode; (b) maximum amplitude of  $B_{1,n}(t)$ , companion mode. —, POD model (3 modes); —, stable conventional Galerkin solutions; ---, unstable conventional Galerkin solutions.

### 8.2. Time domain results

The reduced order model (3 degrees of freedom) built by using time traces “c” gives quite satisfactory results. For this reason, this model has been used to produce the time domain results; the DIVPAG routine of the Fortran library IMSL has been used. The first case studied is with excitation frequency  $\omega/\omega_{1,n} = 0.991$ . All the three proper orthogonal

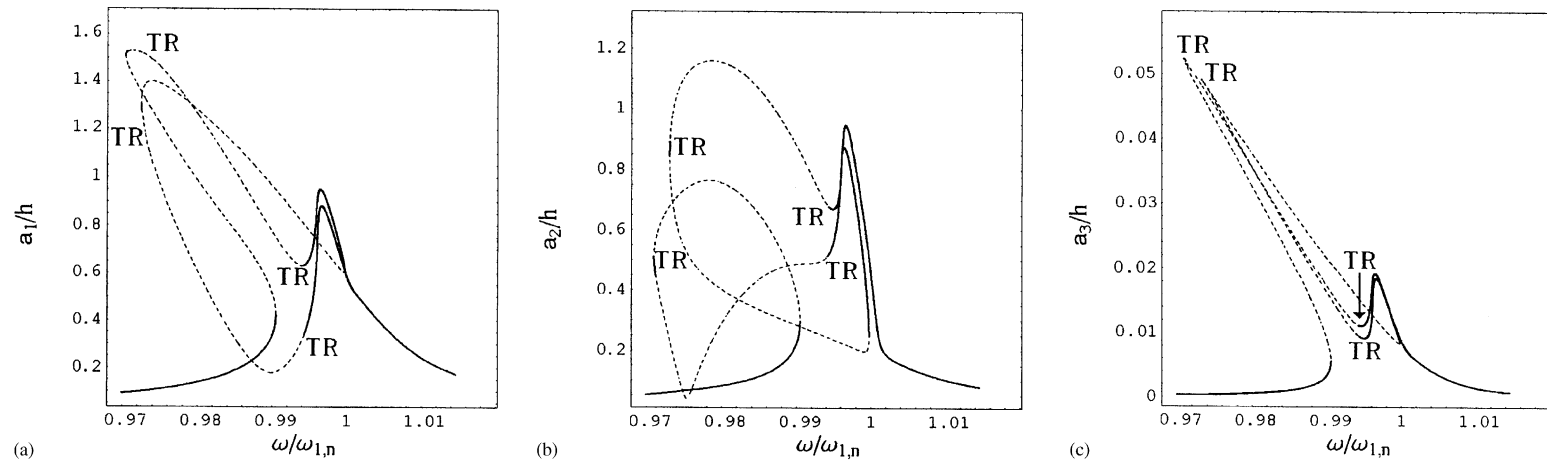


Fig. 12. Maximum amplitude of vibration versus excitation frequency; POD model, case "c". (a) Proper orthogonal coordinate  $a_1(t)$ ; (b) proper orthogonal coordinate  $a_2(t)$ ; (c) proper orthogonal coordinate  $a_3(t)$ . —, stable solutions; ---, unstable periodic solutions.

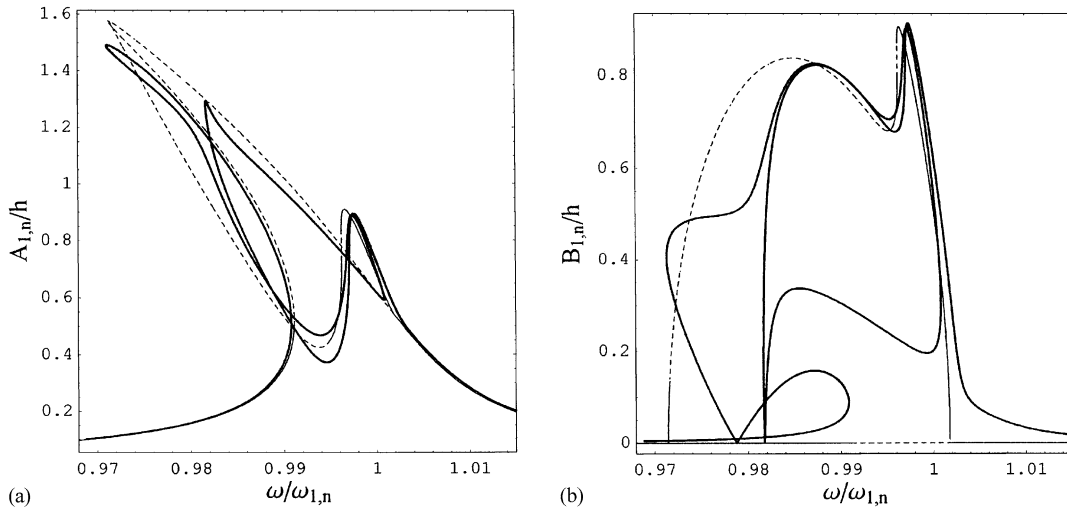


Fig. 13. Maximum amplitude of vibration versus excitation frequency; POD model versus conventional Galerkin model, case “b” (weight 0.3) combined with “d” (weight 0.7). (a) Maximum amplitude of  $A_{1,n}(t)$ , driven mode; (b) maximum amplitude of  $B_{1,n}(t)$ , companion mode. —, POD model (3 modes); ---, stable conventional Galerkin solutions; ···, unstable conventional Galerkin solutions.

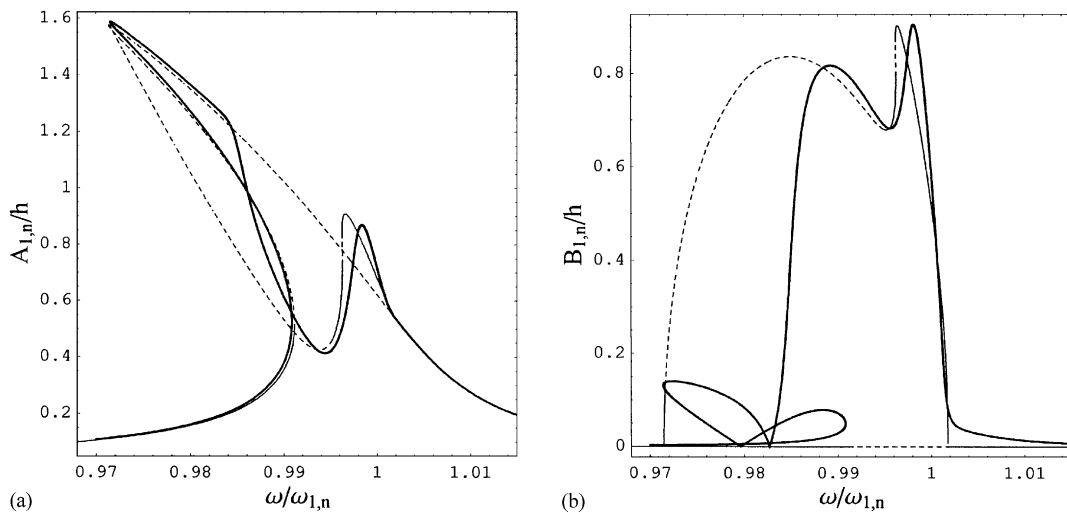


Fig. 14. Maximum amplitude of vibration versus excitation frequency; POD model versus conventional Galerkin model, case “b” (weight 0.5) combined with “d” (weight 0.5). (a) Maximum amplitude of  $A_{1,n}(t)$ , driven mode; (b) maximum amplitude of  $B_{1,n}(t)$ , companion mode. —, POD model (3 modes); ---, stable conventional Galerkin solutions; ···, unstable conventional Galerkin solutions.

coordinates are given in Fig. 18; the most significant modal coordinates are shown in Fig. 19, so that they can immediately, and satisfactorily, be compared to the original time response given in Fig. 4.

The second case investigated is at excitation frequency  $\omega/\omega_{1,n} = 0.995$ . The proper orthogonal coordinates are given in Fig. 20, and the most significant modal coordinates in Fig. 21. The agreement between Fig. 21 and the original time response given in Fig. 5 is particularly good.

**9. Conclusions**

The POD method is a valuable instrument for reducing the dimension of complex nonlinear dynamical systems. However, a reliable model is necessary first, to produce time series of responses in order to obtain the proper orthogonal

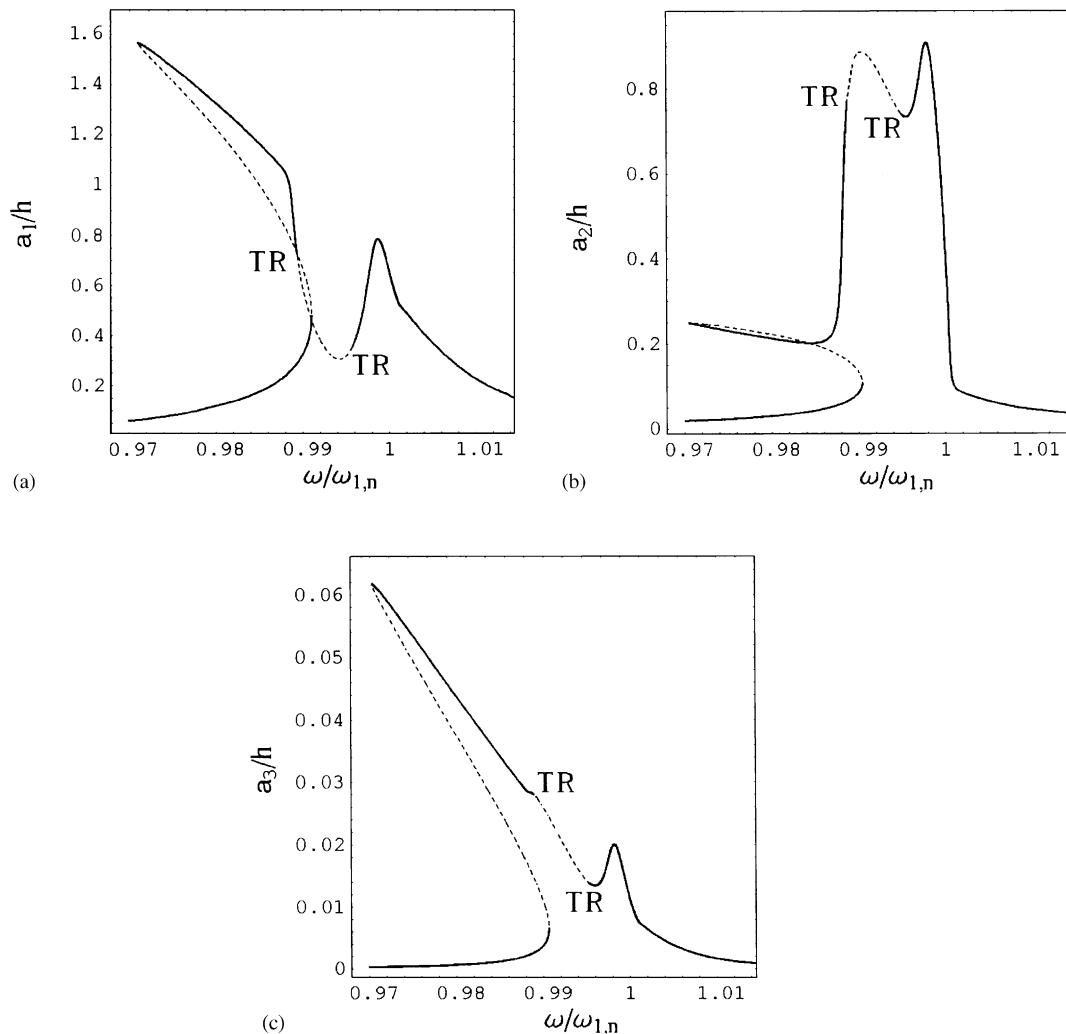


Fig. 15. Maximum amplitude of vibration versus excitation frequency; POD model, case “b” (weight 0.5) combined with “d” (weight 0.5). (a) Proper orthogonal coordinate  $a_1(t)$ ; (b) proper orthogonal coordinate  $a_2(t)$ ; (c) proper orthogonal coordinate  $a_3(t)$ . —, stable solutions; ---, unstable periodic solutions.

modes. Experimental time responses are a possible alternative, but usually they are highly noise-polluted for large-amplitude vibrations. Also, great care must be taken in the choice of appropriate system parameters for which proper orthogonal modes are extracted, in order to capture the essential dynamics of the system for a given parameter range of interest. These aspects, no doubt, limit the practical usefulness of the method.

In the present study the challenging problem of nonlinear (large amplitude) vibrations of a water-filled shell is considered to test the potential of the POD method. In fact, this problem displays behaviour involving simple periodic standing waves, travelling waves and quasiperiodic response in a narrow frequency range around resonance. The system displays a softening-type nonlinearity, with pitchfork and Neimark-Sacker (torus) bifurcations. Qualitatively the shell dynamics is not changed if different dimensions (if the shell is not thick or very long), material properties, or modes excited are considered, and if the fluid contained is eliminated. For this reason, in the present study, different cases have not been considered.

An accurate reduced-order model has been built with only 3 degrees of freedom by using the POD method, versus the 16 degrees of freedom of the original model; (it can be observed that some reduction of the conventional Galerkin model was also possible by eliminating the less significant modes; e.g. see Amabili et al. (1999b, 2000a) and Pellicano et al. (2002). The reduced order model is capable of predicting with good accuracy the vibration amplitude, limit points and both pitchfork and Neimark-Sacker (torus) bifurcations. However, in order to reproduce the pitchfork bifurcations

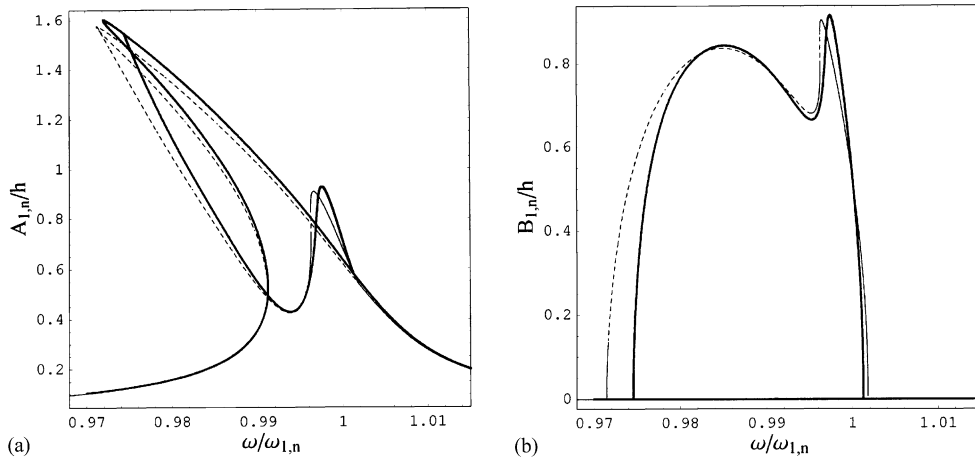


Fig. 16. Maximum amplitude of vibration versus excitation frequency; POD model versus conventional Galerkin model, case “c” (weight 0.5) combined with “-c” (weight 0.5). (a) Maximum amplitude of  $A_{1,n}(t)$ , driven mode; (b) maximum amplitude of  $B_{1,n}(t)$ , companion mode. —, POD model (3 modes); ---, stable conventional Galerkin solutions; ···, unstable conventional Galerkin solutions.

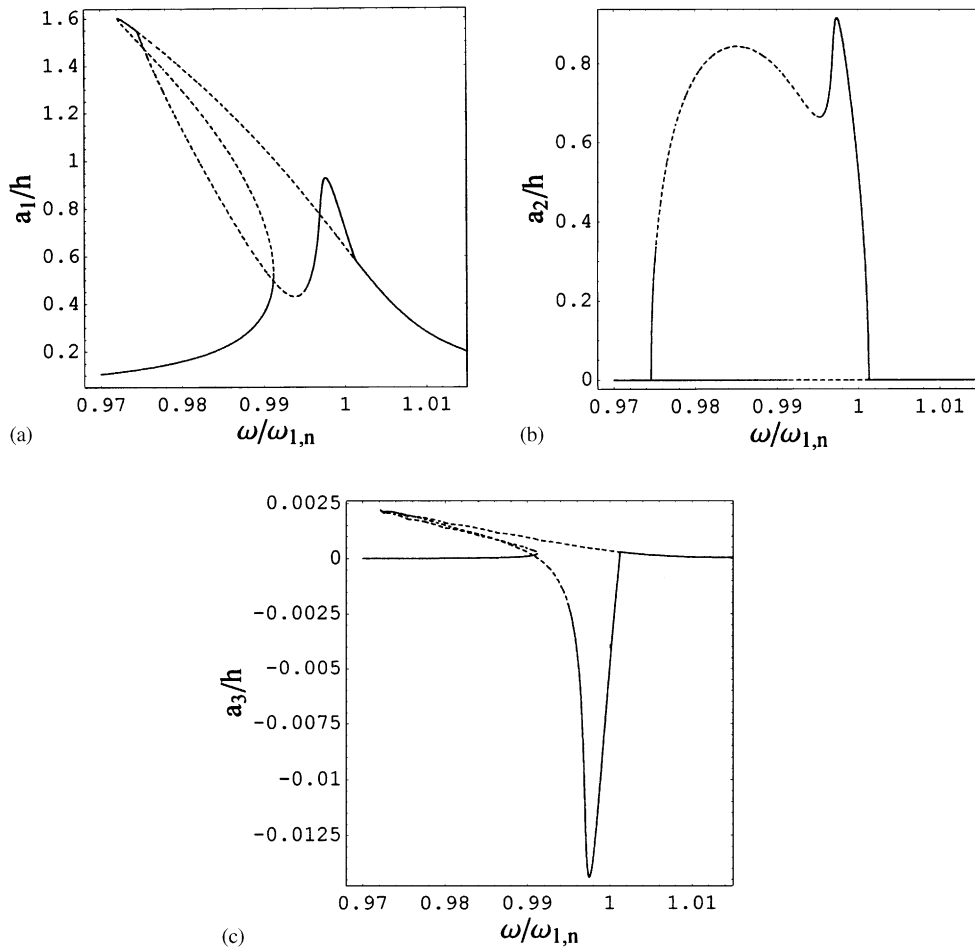


Fig. 17. Maximum amplitude of vibration versus excitation frequency; POD model, case “c” (weight 0.5) combined with “-c” (weight 0.5). (a) Proper orthogonal coordinate  $a_1(t)$ ; (b) proper orthogonal coordinate  $a_2(t)$ ; (c) proper orthogonal coordinate  $a_3(t)$ . —, stable solutions; ---, unstable periodic solutions.

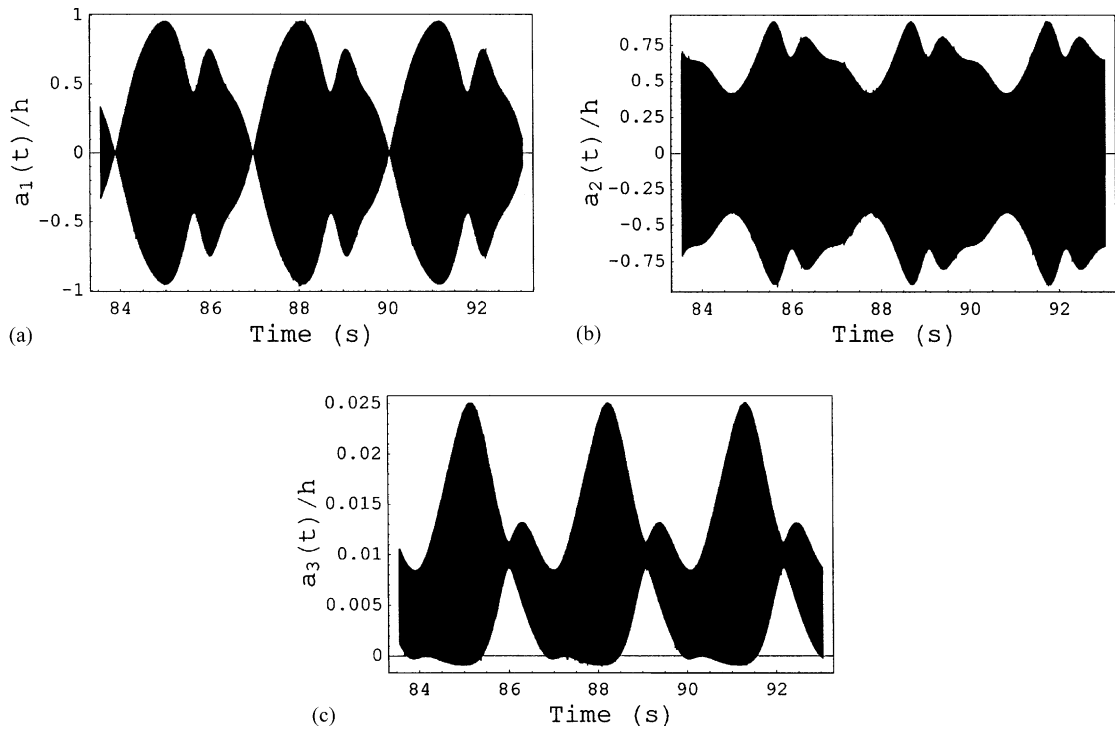


Fig. 18. Time response at excitation frequency  $\omega/\omega_{1,n} = 0.991$ ; POD model, case “c”. (a) Proper orthogonal coordinate  $a_1(t)$ ; (b) proper orthogonal coordinate  $a_2(t)$ ; (c) proper orthogonal coordinate  $a_3(t)$ .

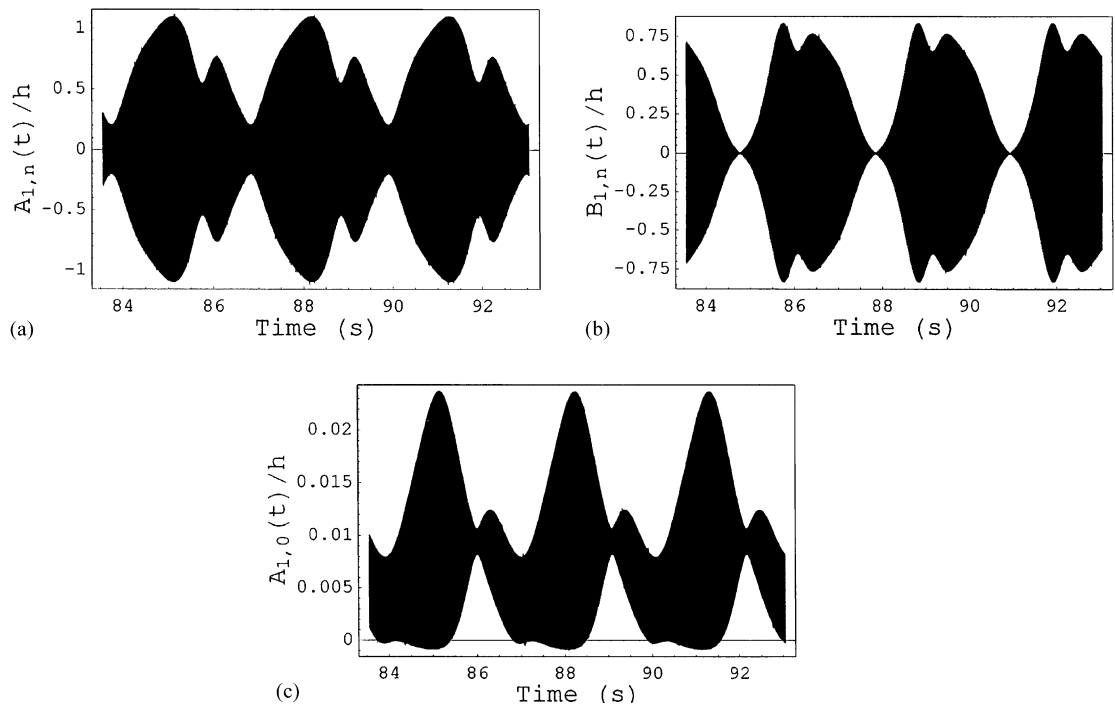


Fig. 19. Time response at excitation frequency  $\omega/\omega_{1,n} = 0.991$ ; POD model, case “c”. (a) Modal coordinate  $A_{1,n}(t)$  associated to the driven mode; (b) modal coordinate  $B_{1,n}(t)$  associated to the companion mode; (c) modal coordinate  $A_{1,0}(t)$  associated to the first axisymmetric mode.

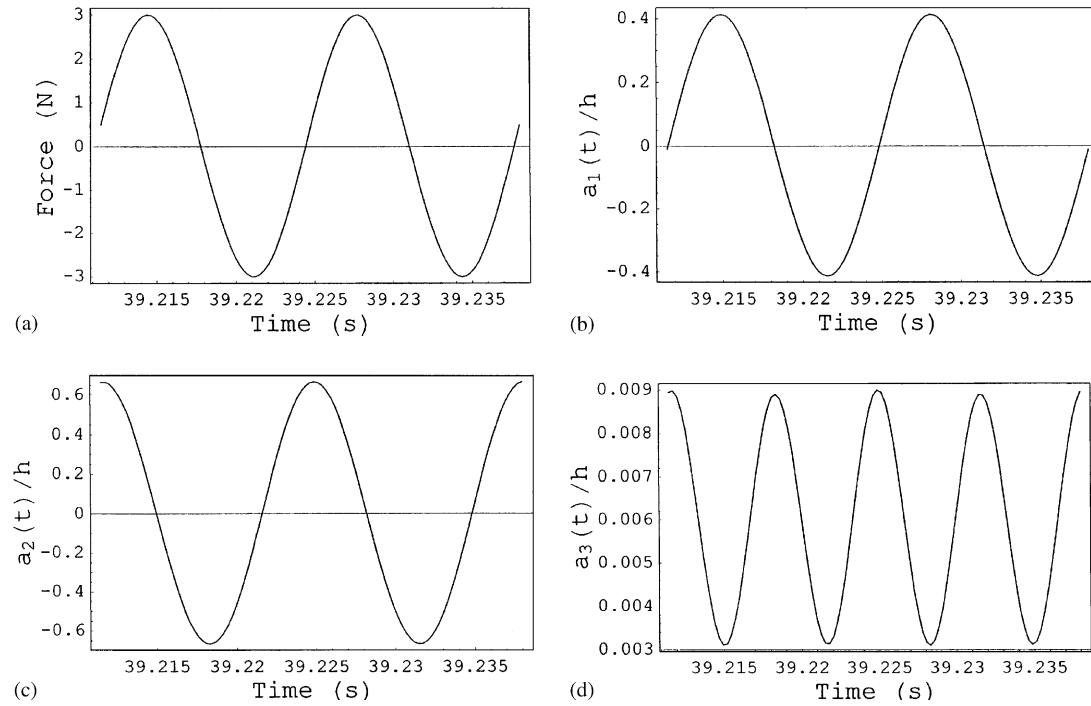


Fig. 20. Time response at excitation frequency  $\omega/\omega_{1,n} = 0.995$ ; POD model, case “c”. (a) Harmonic force excitation; (b) proper orthogonal coordinate  $a_1(t)$ ; (c) proper orthogonal coordinate  $a_2(t)$ ; (d) proper orthogonal coordinate  $a_3(t)$ .

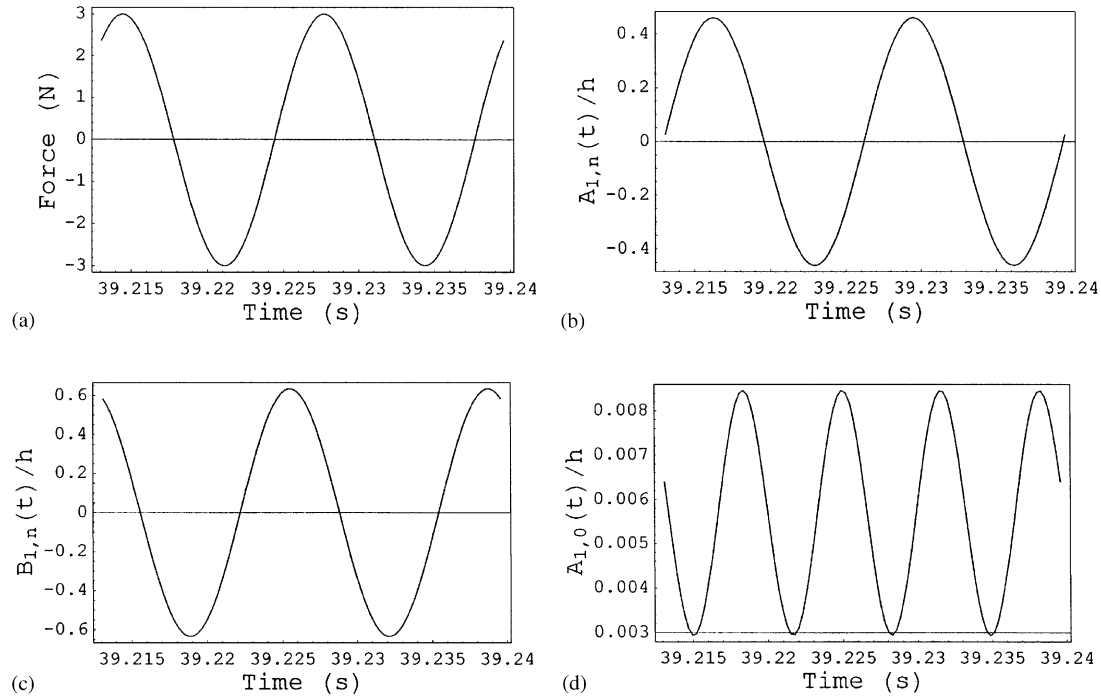


Fig. 21. Time response at excitation frequency  $\omega/\omega_{1,n} = 0.995$ ; POD model, case “c”. (a) Harmonic force excitation; (b) modal coordinate  $A_{1,n}(t)$  associated to the driven mode; (c) modal coordinate  $B_{1,n}(t)$  associated to the companion mode; (d) modal coordinate  $A_{1,0}(t)$  associated to the first axisymmetric mode.

of the original model, it is necessary to utilize both the mirror-image responses, involving travelling waves in opposite directions. The best model has been constructed by using the time response with amplitude modulations obtained for an excitation frequency very close to the fundamental frequency of the water-filled shell.

### Acknowledgements

We acknowledge the valuable suggestion of Professor Arvind Raman of Purdue University concerning the necessity of including responses with travelling waves in opposite directions in order to recover the symmetry of the system (discussion at the “2nd MIT Conference on Computational Fluid and Solid Mechanics”).

This work was partially supported by the FIRB 2001 grant of the Italian Ministry for University and Research (MIUR), NSERC (Canada) and FCAR (Québec).

### References

- Amabili, M., 2003a. Theory and experiments for large-amplitude vibrations of empty and fluid-filled circular cylindrical shells with imperfections. *Journal of Sound and Vibration* 262, 921–975.
- Amabili, M., 2003b. Comparison of shell theories for large-amplitude vibrations of circular cylindrical shells: Lagrangian approach. *Journal of Sound and Vibration* 264, 1091–1125.
- Amabili, M., Païdoussis, M.P., 2003. Review of studies on geometrically nonlinear vibrations and dynamics of circular cylindrical shells and panels, with and without fluid-structure interaction. *Applied Mechanics Reviews* 56 (4), 343–381.
- Amabili, M., Pellicano, F., Païdoussis, M.P., 1999a. Non-linear dynamics and stability of circular cylindrical shells containing flowing fluid. Part I: Stability. *Journal of Sound and Vibration* 225, 655–699.
- Amabili, M., Pellicano, F., Païdoussis, M.P., 1999b. Non-linear dynamics and stability of circular cylindrical shells containing flowing fluid. Part II: Large-amplitude vibrations without flow. *Journal of Sound and Vibration* 228, 1103–1124.
- Amabili, M., Pellicano, F., Païdoussis, M.P., 2000a. Non-linear dynamics and stability of circular cylindrical shells containing flowing fluid. Part III: Truncation effect without flow and experiments. *Journal of Sound and Vibration* 237, 617–640.
- Amabili, M., Pellicano, F., Païdoussis, M.P., 2000b. Non-linear dynamics and stability of circular cylindrical shells containing flowing fluid. Part IV: Large-amplitude vibrations with flow. *Journal of Sound and Vibration* 237, 641–666.
- Aubry, N., Holmes, P., Lumley, J.L., Stone, E., 1988. The dynamics of coherent structures in the wall region of a turbulent boundary layer. *Journal of Fluid Mechanics* 192, 115–173.
- Azeez, M.F., Vakakis, A.F., 2001. Proper orthogonal decomposition (POD) of a class of vibroimpact oscillations. *Journal of Sound and Vibration* 240, 859–889.
- Breuer, K.S., Sirovich, L., 1991. The use of the Karhunen-Loève procedure for the calculation of linear eigenfunctions. *Journal of Computational Physics* 96, 277–296.
- Chen, J.C., Babcock, C.D., 1975. Nonlinear vibration of cylindrical shells. *AIAA Journal* 13, 868–876.
- Doedel, E.J., Champneys, A.R., Fairgrieve, T.F., Kuznetsov, Y.A., Sandstede, B., Wang, X., 1998. AUTO 97: Continuation and Bifurcation Software for Ordinary Differential Equations (with HomCont). Concordia University, Montreal, Canada.
- Dowell, E.H., Ventres, C.S., 1968. Modal equations for the nonlinear flexural vibrations of a cylindrical shell. *International Journal of Solids and Structures* 4, 975–991.
- Evensen, D.A. 1967. Nonlinear flexural vibrations of thin-walled circular cylinders. NASA TN D-4090.
- Ginsberg, J.H., 1973. Large amplitude forced vibrations of simply supported thin cylindrical shells. *Journal of Applied Mechanics* 40, 471–477.
- Gonçalves, P.B., Batista, R.C., 1988. Non-linear vibration analysis of fluid-filled cylindrical shells. *Journal of Sound and Vibration* 127, 133–143.
- Jansen, E.L., 2002. Non-stationary flexural vibration behaviour of a cylindrical shell. *International Journal of Non-Linear Mechanics* 37, 937–949.
- Kubenko, V.D., Koval'chuk, P.S., 1998. Nonlinear problems of the vibration of thin shells (review). *International Applied Mechanics* 34, 703–728.
- Lakis, A.A., Selmane, A., Toledano, A., 1998. Non-linear free vibration analysis of laminated orthotropic cylindrical shells. *International Journal of Mechanical Sciences* 40, 27–49.
- Pellicano, F., Amabili, M., Païdoussis, M.P., 2002. Effect of the geometry on the nonlinear vibrations analysis of circular cylindrical shells. *International Journal of Non-Linear Mechanics* 37, 1181–1198.
- Sarkar, A., Païdoussis, M.P., 2003. A compact limit-cycle oscillation model of a cantilever conveying fluid. *Journal of Fluids and Structures* 17, 525–539.
- Sirovich, L., 1987. Turbulence and dynamics of coherent structures, Part I: coherent structures. *Quarterly of Applied Mathematics* 45, 561–571.
- Wolfram, S., 1999. *The Mathematica Book*, 4th Edition. Cambridge University Press, Cambridge, UK.
- Zahorian, S.A., Rothenberg, M., 1981. Principal component analysis for low-redundancy encoding of speech spectra. *Journal of the Acoustical Society of America* 69, 519–524.